January 2016

Effect Of Nanoclay On Binder Rheology And HMA Rutting Resistance

Daniel David Landrus

EFFECT OF NANOCLAY ON BINDER RHEOLOGY AND HMA RUTTING RESISTANCE

by

Daniel David Landrus
Bachelor of Science, University of North Dakota, 2012

A Thesis
Submitted to the Graduate Faculty

of the

University of North Dakota

in partial fulfillment of the requirements

for the degree of

Master of Science

Grand Forks, North Dakota
May
2016

This thesis, submitted by **Daniel Landrus** in partial fulfillment of the requirements for the Degree of Master of Science in Civil Engineering from the University of North Dakota, has been read by the Faculty Advisory Committee under whom the work has been done and is hereby approved.

Daba Gedafa 5/6/16
Name of Chairperson

5/16/16
Name of Committee Member

for/ Charles Moretti 5/6/16
Name of Committee Member

Name of Committee Member

Name of Committee Member

This thesis is being submitted by the appointed advisory committee as having met all of the requirements of the School of Graduate Studies at the University of North Dakota and is hereby approved.

Wayne Swisher
Dean of the School of Graduate Studies

May 10, 2016
Date

PERMISSION

Title Effect of Nanoclay on Binder Rheology and HMA Rutting Resistance

Department Civil Engineering

Degree Master of Science

In presenting this thesis in partial fulfillment of the requirements for a graduate degree from the University of North Dakota, I agree that the library of this University shall make it freely available for inspection. I further agree that permission for extensive copying for scholarly purposes may be granted by the professor who supervised my thesis work or, in his absence, by the Chairperson of the department or the dean of the School of Graduate Studies. It is understood that any copying or publication or other use of this thesis or part thereof for financial gain shall not be allowed without my written permission. It is also understood that due recognition shall be given to me and to the University of North Dakota in any scholarly use which may be made of any material in my thesis.

5/11/16

Daniel Landrus
Date

TABLE OF CONTENTS

LIST OF FIGURES

LIST OF TABLES

ACKNOWLEDGMENTS

I would like to thank ND EPSCoR and the Graduate School for funding this project.

I would like to thank Strata Corporation, Flint Hills Recourses, and BYK Additives & Instruments for providing the research materials.

I would like to thank my Thesis Committee members Dr. Charles Moretti and Dr. Nabil Suleiman for giving me the guidance support during my time in the master's program at the University of North Dakota.

I would like to extend my deepest gratitude to my Advisor and Thesis Committee Chair, Dr. Daba Gedafa for providing me with endless information and being patient with me during this research.

ABSTRACT

In this study, the change in rheological properties of nanoclay modified asphalt binders was determined in the laboratory. The four performance grade asphalt binders used in this study, PG 58-34, PG 58-28, PG 64-34, and PG 64-28, were modified using Cloisite 20 nanoclay at 1 %, 3%, and 5 % by weight of the asphalt binder. The Dynamic Shear Rheometer (DSR) was used to measure the rheological properties of the unmodified and modified asphalt binders and determine the change in performance properties. The non-modified and modified asphalt binders were also used to create nanoclay modified asphalt specimens using the Superpave Gyratory Compactor (SGC). The rutting resistance of nanoclay modified hot mix asphalt (HMA) specimens were determined using an Asphalt Pavement Analyzer (APA).

The results of the DSR testing show that the nanoclay increases the stiffness of the asphalt. The failure temperature of the asphalt binder generally increased with an increase in nanoclay content. The low-temperature results were interpreted using storage modulus master curves. These master curves showed that the storage modulus increased with an increase in nanoclay. The HMA specimens were tested for rutting resistance using the APA. The results showed that the rutting resistance of HMA specimens based on nanoclay modified asphalt binder was improved as nanoclay content increased. Furthermore there was a better linear correlation with the increase in nanoclay content than there was with the number of gyratory compactor compaction cycles during the preparation of the specimens.

CHAPTER I

INTRODUCTION

Asphalt Pavement Failures

In order to understand why asphalt pavements fail it is necessary to understand how each individual part of the asphalt pavement system works. There are three components of the conventional asphalt pavement system: asphalt pavement, aggregate base course, and the subgrade. Failure of any part of the system causes the system to fail.

Rutting failure is unique to flexible pavements. Poor compaction of any of the pavement and base layers during construction and high temperatures causes rutting. This research paper focuses on modifying the asphalt binder of the pavement to protect against high pavement temperature rutting.

Polymer Modified Asphalt Binder

Modifying the asphalt binder to obtain improved performance is common in asphalt research. Much of the research focuses on using styrene-butadiene-styrene (SBS), elvaloy, ethylene-vinyl-acetate (EVA) and ethylene-styrene-interpolymer (ESI) to improve the properties of the asphalt binder. The research performed for this paper focuses on using Cloisite 20 nanoclay to improve the properties of asphalt binders.

Data Collection

Testing was performed using a Dynamic Shear Rheometer (DSR) to determine the change in rheological properties of binders. The DSR was used to determine the high performance grade temperature rutting resistance of four performance graded asphalt

binders. The four asphalt binders were also tested to determine how the nanoclay modification affected the low-temperature performance properties.

Problem Statement

Rutting resistance of asphalt pavements is the most important performance property to be controlled during the pavement design process. Improper selection of aggregates or binder can result in premature failure.

Focusing on the binder; one can improve pavement rutting resistance by improved binder rutting resistance. The binder rutting resistance can be increased by either increasing the binder stiffness or by decreasing the phase angle of the material. By altering these rheological variables to achieve high temperature rutting resistance the low temperature rheological properties are likely to change. This secondary problem statement was investigated to determine how the low temperature rheological properties change when the binder was modified to achiever the high temperature rutting resistance.

Objectives of Study

Objectives of this research are to:

1. Increase the rutting resistance of asphalt binder with nanoclay modification.
2. Investigate the change in low temperature rheological properties due to the nanoclay modification.
3. Investigate rutting resistance of nanoclay modified HMA specimens at the meso scale.

Organization of Thesis

Chapter I defines rutting resistance and provides background information on how modifying the asphalt binder can mitigate rutting resistance. Chapter II expands on the Chapter I and further describes how asphalt pavement failure occurs. It also provides information on testing for rheological properties of asphalt binders. Chapter III describes material selection, testing procedures, mix designs, HMA properties and data analysis. Chapter IV section documents the results of the research. Finally the conclusions of the research and the recommendations for future testing are made in Chapter V and Chapter VI.

CHAPTER II

LITERATURE REVIEW

Asphalt Cement

Asphalt cement, or asphalt binder, is a dark brown to black cementitious material that is either naturally occurring or produced by petroleum distillation. Almost all of the asphalt cement used in paving applications today is created by the refining of crude oil. At ambient temperatures asphalt cement is a black, sticky, semisolid, and highly viscous material. It is a strong and durable cement that is resistant to most acids, alkalies, and salts. Asphalt cement is primarily used for paving applications in the United States by heating the binder to a liquid state and mixing it with aggregates to form Hot Mix Asphalt (HMA) (Roberts et al. 1996). Asphalt pavement is considered a flexible pavement because it flexes in response to traffic loading.

Asphalt Pavement Distresses

The Federal Highway Administration (FHWA) defines functional and structural pavement failures as follows: functional failure occurs when the pavement is unable to carry out its intended function without causing discomfort to the users and imposing high stress on vehicles due to excess roughness. Structural failure occurs when one or more of the layers of the pavement structure are weakened and are incapable of sustaining the loads imposed on the pavement structure. Asphalt pavements often demonstrate three major types of failure: rutting, low-temperature cracking, and fatigue cracking. These

three pavement distresses can cause functional and structural failure of asphalt pavements and should be carefully considered in the pavement design (Miller et al. 2014).

The most common type of flexible pavement distress is rutting. Rutting is the failure of a flexible pavement due to the permanent deformation in the wheel path of the roadway. Rutting stems from a permanent deformation in any of the pavement layers or in the subgrade. Rutting can also be caused by hot weather or from inadequate compaction during construction. Rutting is created in the wheel paths of traveling vehicles due to secondary compaction of HMA pavement after construction is completed (Huang, 2004). When compaction is poor (10 to 12% or more air voids for a mix designed at 3 to 5%), the channelized traffic provides a repeated kneading action in the wheel track areas and completes the consolidation to the designed air voids level (usually 3 to 5%). A substantial amount of rutting can occur if very thick asphalt layers are consolidated by the traffic (Roberts et al. 1996).

Use of excessive asphalt cement is the most common cause for the rutting phenomenon. Too much asphalt cement in the mix causes a loss of internal friction between aggregate particles and causes the asphalt cement rather than the aggregate structure to carry the loads (Roberts et al. 1996). Plastic flow can be minimized by using large size crushed aggregates and providing adequate compaction at the time of construction. Certain mineral fillers also increase the apparent viscosity of asphalt cement high service temperatures and thus makes the mix more resistant to rutting. Some increased resistance to rutting can be obtained by using stiffer (high viscosity or low penetration) asphalt cements. However, stiffer asphalt cements are more prone to low-temperature cracking during winter in cold regions especially if they are used in the

surface courses (Roberts et al. 1996). The second type of major distress of flexible pavements is low-temperature cracking.

Low-temperature cracking is usually associated with flexible pavements in the Northern regions of the United States and much of Canada, where winter temperatures fall below freezing. Low-temperature cracking is a result of the shrinkage of asphalt pavement during low- temperatures (Huang, 2004). Field observations and measurements have indicated the cracking begins at the surface and progresses down through the asphalt pavement layers over time. This occurs due to low ambient temperatures cooling the asphalt pavement surface first. The asphalt pavement will then develop transverse cracking when the thermal stresses caused by shrinkage are greater than its fracture strength (Roberts et al. 1996). High stiffness of asphalt cement at low temperatures is the predominant cause of this type of cracking. Finally the third major type of flexible pavement distress is fatigue cracking.

The fatigue cracking of flexible pavements is based on horizontal tensile strain at the bottom surface of the HMA layer and can be categorized into two groups: load associated and non-load associated. Load associated fatigue cracking is the fracture under repeated or fluctuating stress. Some of the factors which influence the development of fatigue cracking include: composition of the structural section, asphalt cement consistency, asphalt content, air voids and aggregate characteristics in asphalt mix, in-place properties of untreated aggregates or cement-treated materials, in-place properties of foundation soils, temperature, and traffic loading (Roberts et al. 1996). Non-load associated fatigue cracking is also known as thermal fatigue cracking. Thermal fatigue cracking is similar to the fatigue cracking caused by repeated loading. It is caused by

tensile strain in the asphalt layer that is due to daily temperature cycle. Thermal fatigue cracking can occur in much milder regions if an excessively hard asphalt is used or the asphalt becomes hardened by aging. Table 1 shows a summary of the pavement distresses and causes of failure.

Table 1: Causes of Flexible Pavement Failure

Asphalt Pavement Failure Type	Causes of Failure
Rutting:	Excessive Asphalt Binder Content Poor Compaction Rounded Aggregate Low Asphalt Binder Stiffness
Low-Temperature Cracking:	High Asphalt Binder Stiffness Low Elasticity High Asphalt Binder Content
Fatigue Cracking:	High Asphalt Binder Stiffness Low Elasticity

Strategic Highway Research Program Specifications (SHRP)

SHRP launched in 1987 to develop performance based tests and specifications for asphalt binders and HMA mixtures. Since this time, SHRP researchers have determined that with every traffic loading cycle, work was being done on the HMA to deform it. Part of this work was recovered by the elastic rebound of the HMA and some of the work was non-recoverable. To minimize permanent deformation in the form of rutting, the amount

of work dissipated during each cycle should be minimized. Equation 1 was developed to determine the work dissipated per loading cycle (Roberts et al. 1996).

Equation 1: Work Dissipated Due to Applied Stress

$$W_c = \pi \times \sigma_0^2 \left[\frac{1}{G^*/\sin\delta}\right]$$

Where,

W_c=work dissipated per load cycle,

σ_0=stress applied during the load cycle,

G^*=Complex Modulus

δ=Phase Angle

The equation shows that in order to reduce rutting, the complex modulus can be increased or the phase angle can be decreased. SHRP researchers also developed an equation to investigate the fatigue cracking resistance of asphalt binders (Roberts et al. 1996). Equation 2 shows that fatigue cracking can be reduced by decreasing G* or δ. As G* decreases the elasticity of the asphalt binder increases allowing it to deform without building up large stresses. A low δ corresponds to elastic material that can deform and regain its original shape without dissipating work.

Equation 2: Work Dissipated Due to Applied Strain

$$W_c = \pi \times \varepsilon_0^2 \left[G^* \times \sin\delta\right]$$

Where all other variable are the same as previously described and;

ε=strain

Work can be dissipated in several ways: heat dissipation, plastic flow (rutting), cracking, and crack propagation. Heat dissipation is the creation of heat due to movement of pavement particles during loading. This loading also permanently deforms the pavement structure beyond the yield stress. The cyclic loading of the pavement will

eventually create a crack in the bottom surface of the asphalt pavement. This crack will then propagate with each additional loading cycle (Huang, 2004).

Superpave Classification

The most popular method of classifying asphalt binders today is the Superpave asphalt binder specification. The Superpave binder specification is based on the physical properties of asphalt binder and the temperature at which the properties are achieved. The notation for the Superpave binder specification is PG 64-28. This reads "performance grade sixty-four minus twenty-eight" and describes the climate at which this binder performs best. The first set of numbers determines the seven day average high temperature of the pavement being 64°C. The second set of numbers determines the likely single day low pavement temperature being -28°C (Roberts et al. 1996). Both the high temperature and low temperature criteria to determine the Superpave classifications are determined using the rheological properties of asphalt binders.

Asphalt Binder Rheological Properties

There are four important rheological properties of asphalt binders that relate to the performance of asphalt pavements and the susceptibility of flexible pavements to failure. These four rheological properties are age hardening, temperature susceptibility, shear susceptibility, and stiffness (Roberts et al. 1996).

The first rheological property is age hardening. During the construction process of HMA pavements, the first significant hardening of asphalt cement takes place in a drum mixer where the heated aggregate is mixed with hot asphalt binder. During the mixing time, the asphalt is in very thin films and is exposed to high temperatures (275 - 325°F), which cause rheological changes from both oxidation and loss of more volatile

components in the asphalt cement thus increasing the stiffness of the asphalt binder. Age hardening of the asphalt cement continues through processing, transportation to the paving site, placing, and, finally, compacting the HMA mixture. After the pavement has cooled and has been opened to traffic, the age hardening process continues at a significantly slower rate (Huang, 2004).

Asphalt cement is a thermoplastic material, and therefore, its consistency changes with changes in temperature. Asphalt binders that are highly susceptible to temperature are not desirable because a low viscosity at high temperature results in rutting vulnerability. Similarly, a very high viscosity at low temperature results in low temperature shrinkage of the pavement causing low temperature cracking of the HMA (Huang, 2004).

At high temperatures most asphalt cements behave like a Newtonian fluid. This means that they display purely viscous flow in which the rate of shear strain is proportional to stress; viscosity is independent of shear rate. At low temperatures and after aging, the asphalt binder behaves like a non-Newtonian fluid or viscoelastic fluid. Non-Newtonian fluids have a viscosity that is dependent on the shear rate. At very short loading time and/or low temperature, the HMA behaves like an elastic material. At longer loading times and higher temperatures, the stiffness of the asphalt binder demonstrates a relationship between the applied stress and the resulting strain. Therefore, the higher the shear rate is the higher the viscosity or stiffness of the asphalt binder is. This explains the relationship between slow moving vehicles causing greater damage to flexible pavements than faster moving vehicles (Roberts et al. 1996).

Dynamic Shear Rheometer (DSR)

The DSR is used to characterize the viscous and elastic behavior of asphalt binders. Rheology is the study of how matter flows. The focus on rheological properties of asphalt binders is used to determine the stress-strain behavior of the asphalt binder, as well as, relate it to the performance of the asphalt pavement. The principle used within the DSR is to apply sinusoidal, oscillatory stresses and strains to a thin disc of asphalt binder that is sandwiched between the two parallel plates of the DSR. Normally, DSR tests are conducted over a range of temperatures and loading frequencies in order to provide a complete characterization of the viscoelastic properties of the binder (Airey et al. 2004). The DSR can measure the complex shear modulus (|G*|) and phase angle (δ). (|G*|) is defined as the ratio of maximum (shear) stress to maximum strain and provides a measure of the total resistance of the asphalt binder to deformation when the bitumen is subjected to repeated shear loading. Figure 1 shows that the complex modulus is made up of two components: the storage modulus (G') and the loss modulus (G"). The storage modulus is the elastic or recoverable part of the deformation resistance while the loss modulus is the viscous or non-recoverable portion (Roberts et al. 1996).

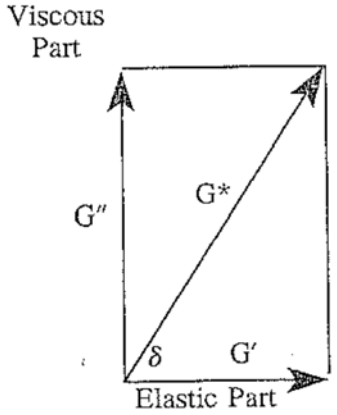

Figure 1: Complex Modulus (Roberts et al. 1996)

Both temperature and loading rate impact the values for |G*| and δ of asphalt binders. Asphalt binders behave like an elastic solid at low temperatures and behave like a viscoelastic material at service temperatures. When the viscoelastic asphalt binder is loaded the elastic deformation is recovered while the viscous deformation is lost. Figure 2 shows that the phase angle is the lag time between applied shear stress and the shear strain response. A 0° phase angle corresponds to a perfectly elastic material, this means that there is an immediate response to an applied stress. A 90° phase angle corresponds to a viscous fluid (Roberts et al. 1996)

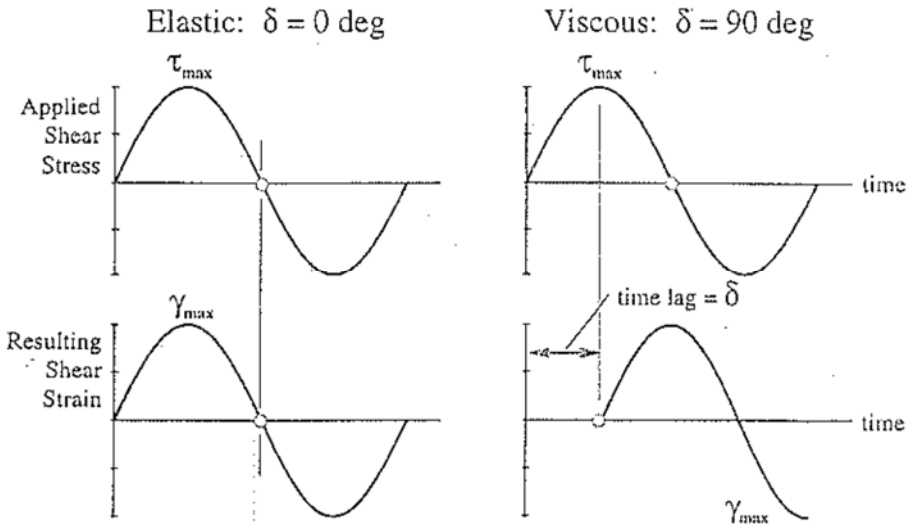

Figure 2: Elastic and Viscous Phase Angle (Roberts et al. 1996).

Nanoclay Modified Asphalt Binders

The purpose of using polymer modified asphalt binders is to achieve desired engineering properties. These properties include but are not limited to: increased shear modulus, reduced plastic flow at high temperatures, and increased resistance to low-temperature cracking. There are many polymer modifiers that will achieve desired engineering properties, but there are several variables to consider when selecting an

asphalt binder modifier. These variables include the desired rheological benefit, chemical compatibility with the base asphalt binder, and mixing times and temperatures (Newman, 1998). The engineering properties of asphalt cement and polymer modified asphalt cements can be determined using the DSR.

One study performed by Yao et al. (2013) showed it is possible to improve rutting resistance and fatigue cracking resistance of asphalt binders by using montmorillonite nanoclay as a mineral additive. The nanoclay modifiers used in this study were both non-modified nanoclay (NMN) and polymer modified nanoclay (PMN). These modifiers were added to the control binder at 2% and 4% concentrations by weight of the asphalt binder. The modified binders were then prepared in a high shear mixing machine at 130°C and 4000 rpm for two hours. Following this, the modified asphalt binders were tested to determine the rheological properties.

Yao et al. (2013) concluded that the addition of NMN in the control asphalt binder makes the material stiffer. High complex shear modulus and rutting factor of these modified asphalt binders reveal that asphalt binder can reflect more energy when loading is applied. The modified NMN binder have more resistance to rutting and fatigue cracking under high and intermediate temperatures. Despite this, the recovery ability of these NMN asphalt binders may be reduced due to the increased stiffness. The addition of the PMN was found to be the exact opposite of NMN. Therefore the high and intermediate temperature resistance to rutting and fatigue was lowered, but the low temperature recovery ability was increased. This shows that NMN modified asphalt binders can be used to increase the rutting resistance and lower the fatigue susceptibility

of asphalt pavements. Also, the use of PMN modifying of asphalt binders can increase the elasticity of asphalt pavements reducing the low-temperature cracking susceptibility.

A similar investigation of nanoclay modified asphalt binders was completed by Onochie et al. (2012). This investigation determined that the addition of nanoclay to modify binders led to an increase in viscosity, aging resistance, and high temperature performance due to an increase in asphalt binder stiffness.

Another study by Nazal et al. (2012) investigated why the nanoclay modified asphalt binders increased rheological properties. They determined that using nanoclay as a modifier increased the stiffness and hardness of the asphalt binder through the development of a rigid network consisting of nanoclay particles and asphaltene aggregates within the composites.

Linear Viscoelastic Limits of Bituminous Binders

To be able to predict the engineering performance of a material it is necessary to understand the stress strain behavior of the material. The stress-strain relationships of viscoelastic materials, such as asphalt binders, are intermediate between the behavior of an elastic solid and a viscous fluid. Asphalt binders display nonlinear stress-strain behavior with nonlinearity only becoming negligible at small strains. These small strains occur within the Linear Viscoelastic (LVE) region. The LVE region is defined in terms of the constitutive relationship between the stress and strain. Asphalt binders must obey two simultaneous conditions to be considered linear viscoelastic: one, the homogeneity (proportionality) condition is obeyed, and two, the linear superposition principle holds (Marasteanu 1999). When data is collected within the LVE range; the asphalt binder's stress strain relationship is only influenced by temperature and loading time but not by

the magnitude of the stress or strain. Viscoelastic parameters of complex modulus, phase angle, storage modulus, and loss modulus are defined under LVE conditions.

Generally speaking asphalt binders have a wide range in which they have a linear stress strain relationship. It is very important to perform the DSR testing within the LVE range to ensure that the results obtained through testing will not be influenced by nonlinear relationships. Unmodified asphalt binders are considered to be thermo-rheological simple materials making time-temperature superposition principle is true within the limits of the linear viscoelastic region (Marasteanu et al 2000).

DSR research performed by SHRP on non-modified asphalt binders found the shear stress and strain LVE limits to be the function of complex modulus as defined Equations 3 and 4 (Anderson et al. 1994).

Equation 3: LVE Limit: Shear Strain

$$\gamma=12.0/(G^*)^{0.29}$$

Equation 4: LVE Limit: Shear Stress

$$\tau=0.12(G^*)^{0.71}$$

The LVE linearity limit was defined by SHRP as the point where the complex modulus has decreased to ninety-five percent of its initial value (Anderson et al. 1994).The SHRP studies did not include modified binders. Research performed by Airey et al. (2004) used non-modified, polymer modified, and process modified asphalt binders to determine the effects of modification on LVE linearity limits, both plastomeric and elastomeric polymer modifiers were used to create the polymer modified asphalt binders. The research completed by Airey et al. (2004) concluded that only elastomeric polymer

modified asphalt binders showed any significant differences in linearity limits and rheological properties when compared to conventional materials.

Marasteanu and Anderson (2000) developed a check for linearity of DSR data. They proposed that if the value of complex modulus did not drop more than five percent of the initial value, linearity conditions were considered to be valid. This corresponds with homogeneity (proportional) condition proposed by (Marasteanu (1999). To check that the linear superposition principle holds, Marasteanu and Anderson (2000) proposed that multiwave single-point tests be performed to obtain the complex shear modulus and phase angle values for each of the component individual waveforms used to create the multiwave signal. The results from the multiwave single point tests for complex modulus and phase angle should equal the sum of the individual single point tests. Results that show differences in values more than five percent show that the superposition principle is not valid.

The research completed in this study conformed to the first condition of linear viscoelastic materials. The complex modulus results obtained in this research did not vary more than five percent from the initial value. The second condition of viscoelastic materials, principle of superposition, was assumed valid. This assumption was based on visual analysis of storage modulus master curves.

Low-Temperature Rheological Properties

DSR testing has previously been used for only high and intermediate temperatures but is able to determine low temperature behavior of asphalt binder. Low temperature specification performance grade test are usually performed on the Bending Beam Rheometer (BBR) using AASHTO T313 or AASHTO PP42. This requires a sample size

approximately 15 grams of binder per beam. There is now alternative low temperature mechanical tests performed on the DSR that uses only approximately 25 milligrams of binder.

The new procedure used 4 mm parallel plates on a DSR and machine compliance for testing of binder properties as low as -40° was developed by the Western Research Institute with the support of the Turner-Fairbank Highway Research Center (Sui et al. 2010). This new procedure allows for small scale sampling and intermediate temperature sample preparation. DSR testing was completed and compared to BBR data to determine the correlation between the data sets. The DSR testing using 4 mm diameter parallel-plates combined with a machine compliance correction was used to measure the low-temperature properties of asphalt binders. Master curves were generated from isotherms in a temperature range from -40 to 30 °C (Sui et al. 2010)

The low temperature specification from the DSR was determined through the establishment of a correlation between the BBR creep stiffness and the shear stress relaxation modulus from the DSR as well as between the corresponding apparent relaxation rates. A strong linear relationship between BBR and DSR data was observed. The coefficient of correlation for creep stiffness vs. shear relaxation modulus and apparent relaxation rate (BBR) vs. apparent relaxation rate (DSR) were 0.986 and 0.957, respectively (Sui et al. 2010)

Machine compliance is needed to ensure that data is collected inside the LVE range. When the rheometer is cooling the specimen down to the low performance grade temperature of the asphalt binder, the components of the measuring system also cool and

deform due to the change in temperature. Equations 5 and 6 show the importance of machine compliance (Sui et al. 2010).

Equation 5: Machine Compliande: Complex Modulus

$$G = \tau/\gamma$$

Equation 6: Machine Compliance: Measured Shear Strain

$$\gamma_{measured} = \gamma_{sample} + \gamma_{instrumnet} = \frac{\tau}{G_{sample}} + \frac{\tau}{G_{instrument}}$$

Where:

G = Shear Modulus

τ = Shear Stress

γ = Shear Strain (deformation)

Equation 6 shows that at high temperatures the modulus of the sample is negligible compared to the modulus of the measuring tool (aluminum or stainless steel) therefore the deformation due to the second term is negligible. When testing at low temperatures the second term is no longer negligible and results in a measured modulus of the sample is lower than its true value. The machine compliance can be corrected for and the measured modulus will better represent the true value (Sui et al. 2010)

CHAPTER III

RESEARCH METHODOLOGY

Material Selection

Unmodified asphalt binders designated as PG 64-34, PG 64-28, PG 58-34, and PG 58-28 were donated by Flint Hills Resources. These binders were chosen for this research because they are the most commonly used asphalt binders used in the Midwest. This was done for two reasons, applicability and availability. This research should be able to provide data and results that can be used in engineering practice in the Midwest. These binder grades are also used in high quantities in the Midwest which will make future research materials easily obtainable.

Cloisite 20 Nanoclay was chosen because of the design of the Nanoclay and the cost. Cloisite 20 is an organic Nanoclay that is designed for thermoplastics. The Nanoclay, when properly dispersed in the thermoplastic system, will create a strong three dimensional network that will improve the neat distortion temperature, improve barrier characteristics and improve retardation performance. The performance of the thermal-plastic systems can improve up to five times with three percent by weight Nanoclay Cloisite 20 added to the system. The assumption is that the thermal-plastic additive will help the asphalt binder perform better against rutting at high temperatures by using the creation of the three dimensional network of Nanoclay. This will provide additional strength against loading. This material was also distributed to the University of North Dakota for research at no cost.

Rheology of Modified and Non-Modified Binders

The DSR test followed AASHTO T 315 standard for determining rutting resistance. The binder was subjected to shear stress for a range of temperatures ranging from PG - 6°C to PG + 6°C. This test determined binder stiffness (G*), phase angle (δ), storage modulus (G'), loss modulus (G"), and shear stress (τ). A 10% strain rate and frequency of 10 rad/sec is assigned for all DSR test. At each temperature, 20 points are measured and the values for G*, δ, τ, and recorded. The Rheocompass software also calculates and records the Superpave rutting parameter.

The proposed standard by Western Research Institute with the support of the Turner-Fairbank Highway Research Center was used to determine the low temperature specification performance grade properties. This test determined complex modulus (G*) and phase angle (δ). Master curves of G* and δ at selected temperatures can be developed to calculate low temperature performance properties.

The specimens used in this Dynamic Shear Rheometer test are created, loaded and trimmed, using the same procedure as above using a 4 mm diameter silicon mold. The specimen was then loaded and conditioned at 30°C for 20 minutes. The temperature was then lowered to the performance temperature of the asphalt binder and conditioned for an additional 20 minutes. The testing then consisted of a strain sweep to determine the LVE range. The Rheometer then performs a frequency sweep from 0.1 to 50 radians per second using the linear strain determined in the strain sweep. This procedure is repeated at 10°C and 20°C above the performance grade of each asphalt binder.

HMA Mix Design

The HMA mix design was based off of AASHTO MP2 standard specification for Superpave volumetric mix design. Table 2 shows the sieve analysis for 1/2 inch nominal size aggregate. This table was the basis for the two job mix formulas that were created. Table 3 and Table 4 show the job mix formulas.

Table 2: AASHTO MP2

		Control Points		Restricted Zone	
Sieve Size	Sieve Size No.	Lower	Upper	Lower	Upper
19 mm	3/4"	100	-	-	-
12.5 mm	1/2"	90	100	-	-
9.5 mm	3/8"	-	90	-	-
4.75 mm	No. 4	-	-	-	-
2.36 mm	No. 8	28	58	39.1	39.1
1.18 mm	No. 16	-	-	25.6	31.6
0.60 mm	No. 30	-	-	19.1	23.1
0.30 mm	No. 50	-	-	15.5	15.5
0.15 mm	No. 100	-	-	-	-
0.075mm	No. 200	2	10	-	-

The individual aggregate sieve analyses are found in the Appendix. Asphalt binder was added to the aggregate at 6% of the total aggregate weight.

Table 3: Job Mix Formula 1

eve Size No.	Blend Percentages				Specifications		Final Mix Proportions
	0.45	0.3	0.2	0.05			
	Agg: D	Agg: A	Agg: B	Agg: F	Min	Max	
1"	0.45	0.30	0.20	0.05	-	-	100.00%
3/4"	0.45	0.30	0.20	0.05	100.00%	-	100.00%
1/2"	0.42	0.30	0.20	0.05	79.00%	99.00%	96.52%
3/8"	0.30	0.30	0.20	0.05	68.00%	88.00%	85.37%
No. 4	0.03	0.26	0.20	0.05	48.00%	68.00%	54.17%
No. 8	0.01	0.20	0.20	0.05	33.00%	53.00%	45.68%
No. 16	-	0.14	0.18	0.05	20.00%	40.00%	37.12%
No. 30	-	0.08	0.13	0.05	14.00%	30.00%	26.83%
No. 50	-	0.03	0.05	0.05	9.00%	21.00%	13.09%
No. 100	-	0.02	0.01	0.05	6.00%	16.00%	7.49%
No. 200	-	-	-	0.04	3.00%	6.00%	4.17%

Table 4: Job Mix Formula 2

Sieve Size No.	Blend Percentages					Specifications		Final Mix Proportions
	0.25	0.2	0.3	0.2	0.05			
	Agg: G	Agg: H	Agg: A	Agg: B	Agg: F	Min	Max	
1"	0.25	0.20	0.30	0.20	0.05	100.00%	-	100.00%
3/4"	0.24	0.20	0.30	0.20	0.05	90.00%	100.00%	99.20%
1/2"	0.16	0.20	0.30	0.20	0.05	79.00%	99.00%	91.43%
3/8"	0.10	0.20	0.30	0.20	0.05	68.00%	88.00%	85.24%
No. 4	0.01	0.01	0.26	0.20	0.05	48.00%	68.00%	53.15%
No. 8	0.00	0.00	0.20	0.20	0.05	33.00%	53.00%	45.17%
No. 16	-	-	0.14	0.18	0.05	20.00%	40.00%	37.12%
No. 30	-	-	0.08	0.13	0.05	14.00%	30.00%	26.83%
No. 50	-	-	0.03	0.05	0.05	9.00%	21.00%	13.09%
No. 100	-	-	0.02	0.01	0.05	6.00%	16.00%	7.49%
No. 200	-	-	-	-	0.04	3.00%	6.00%	4.17%

HMA Compaction

The HMA specimens were created with a Superpave Gyratory Compactor (SGC) using AASHTO T 312. After the asphalt mixture is thoroughly mixed and completed the short term aging of 2-4 hours the mixture is ready to be compacted. A compaction mold and end plates are placed in an oven at the required compaction temperature to pre-heat the mold and end plates to compaction. When the bituminous mixture is within the compaction temperature range, remove the heated mold and end plate from the oven and place a paper disc in the bottom of the mold. Pour the pre-weighed quantity of asphalt mixture into the mold and level off the top surface. Place another paper disc on top of the asphalt mixture. The mold is then loaded into the SGC. The machine will lower the ram

until the pressure on the specimen reaches 600 kPa, apply a 1.25º average internal angle to the mold assembly and begin the gyratory compaction. Allow the compaction to proceed until the desired specimen height is reached and the ram retracts. Record the specimen height and number of compaction gyrations. Extrude the specimen from the mold and remove the paper discs.

The table below 5 lists the mixture quantities and HMA specimen data. The SGC was set to stop gyratory compaction at a specimen height of 75 mm. The proportions of the HMA were set during a trial and error process to obtain a desired 75 gyrations.

Table 5: HMA Specimen Data

Job Mix Formula 1: Target Mix Proportions						
Agg D (g)		Agg A (g)	Agg B (g)	Agg F (g)	Binder (g)	Total (g)
1316.25		877.5	585	146.25	175.5	3100.5
Job Mix Formula 2: Target Mix Proportions						
Agg G (g)	Agg H (g)	Agg A (g)	Agg B (g)	Agg F (g)	Binder (g)	Total (g)
767	613	920	613	153	184	3250

It is important to note that two different mix designs were used throughout this research. PG 64-28 and PG 58-34 HMA specimens were created using Job Mix Formula 1. PG 64-34 and PG 58-28 HMA specimens were created using Job Mix Formula 2 The comparison of results should not extend across all binders. The HMA were then tested to determine volumetric properties. The following table shows the volumetric properties of the HMA specimens.

Table 6: HMA Volumetric Properties

Specimen ID	Weight (g)	SSD Weight (g)	Submerged Weight (g)	Bulk Specific Gravity (Gmb)	Rice Specific Gravity (Gmm)	% Air Voids (Va)
PG 64-34-5%-3	3195.8	3201.2	1876.1	2.412	2.47	2.35
PG 64-34-5%-2	3259.8	3261.2	1923.6	2.437	2.47	1.32
PG 64-34-5%-1	3218.7	3222.2	1898	2.431	2.47	1.58
PG 64-34-3%-3	3240.5	3242.3	1913.8	2.439	2.54	3.96
PG 64-34-3%-2	3237.8	3240.2	1912.2	2.438	2.54	4.01
PG 64-34-3%-1	3242.7	3244.8	1914.5	2.438	2.54	4.03
PG 64-34-1%-3	3289.2	3291.8	1943.9	2.440	2.49	1.89
PG 64-34-1%-2	3225.3	3226.8	1903	2.436	2.49	2.04
PG 64-34-1%-1	3245.6	3247.8	1919.3	2.443	2.49	1.78
PG 64-34-0%-3	3292.3	3294.1	1940.9	2.433	2.44	0.41
PG 64-34-0%-2	3238.9	3241	1912.6	2.438	2.44	0.20
PG 64-34-0%-1	3192.4	3196.3	1874.9	2.416	2.44	1.11
PG 64-28-5%-3	3160.2	3162.9	1847.4	2.402	2.49	3.57
PG 64-28-5%-2	3194.6	3199	1871	2.406	2.49	3.44
PG 64-28-5%-1	3130.4	3137.5	1821.9	2.379	2.49	4.49
PG 64-28-3%-3	3171.4	3175.8	1853.1	2.398	2.50	4.05
PG 64-28-3%-2	3119.6	3125.2	1817.5	2.386	2.50	4.54
PG 64-28-3%-1	3152.3	3156.1	1838.9	2.393	2.50	4.23
PG 64-28-1%-3	3147.6	3150.8	1834	2.390	2.50	4.26
PG 64-28-1%-2	3150.8	3154.4	1838.7	2.395	2.50	4.08
PG 64-28-1%-1	3149.9	3153.9	1841.4	2.400	2.50	3.87
PG 64-28-0%-3	3092.8	3098	1805.4	2.393	2.48	3.62
PG 64-28-0%-2	3121.5	3124.4	1820.4	2.394	2.48	3.58
PG 64-28-0%-1	3129.5	3132.9	1834.3	2.410	2.48	2.93
PG 58-34-5%-3	3164.5	3168.8	1843.4	2.388	2.51	4.79
PG 58-34-5%-2	3120.3	3132.1	1806.8	2.354	2.51	6.11
PG 58-34-5%-1	3185	3190.9	1862.1	2.397	2.51	4.42
PG 58-34-3%-3	3161.4	3166.7	1842.5	2.387	2.46	3.14
PG 58-34-3%-2	3232.7	3235.8	1896.5	2.414	2.46	2.07
PG 58-34-3%-1	3081.1	3092.5	1770.7	2.331	2.46	5.43
PG 58-34-1%-3	3187.3	3190.1	1862	2.400	2.43	1.17
PG 58-34-1%-2	3097	3109.6	1786.6	2.341	2.43	3.60
PG 58-34-1%-1	3152	3155.6	1826.4	2.371	2.43	2.35
PG 58-34-0%-3	3140.5	3145.3	1828.5	2.385	2.45	2.82
PG 58-34-0%-2	3123.1	3129.2	1809.9	2.367	2.45	3.54
PG 58-34-0%-1	3141.5	3146.3	1827.1	2.381	2.45	2.97
PG 58-28-5%-3	3191.6	3195	1871.7	2.412	2.49	3.05
PG 58-28-5%-2	3147.3	3155.8	1841	2.394	2.49	3.77

Table 6 cont.

Specimen ID	Weight (g)	SSD Weight (g)	Submerged Weight (g)	Bulk Specific Gravity (Gmb)	Rice Specific Gravity (Gmm)	% Air Voids (Va)
PG 58-28-5%-1	3177.1	3183.3	1864.9	2.410	2.49	3.13
PG 58-28-3%-3	3111	3123.7	1802.1	2.354	2.49	5.61
PG 58-28-3%-2	3161.2	3166.4	1854.3	2.409	2.49	3.39
PG 58-28-3%-1	3161.2	3168.4	1850.4	2.398	2.49	3.82
PG 58-28-1%-3	3134.4	3141.6	1823.7	2.378	2.48	4.13
PG 58-28-1%-2	3097.7	3104.3	1802	2.379	2.48	4.12
PG 58-28-1%-1	3140.8	3147.8	1824.3	2.373	2.48	4.34
PG 58-28-0%-3	3172.7	3177.5	1853.2	2.396	2.45	2.25
PG 58-28-0%-2	3156.8	3164.7	1845.1	2.392	2.45	2.39
PG 58-28-0%-1	3127.3	3135.4	1812.3	2.364	2.45	3.56

The Rice Specific Gravity was determined using AASHTO T 209 standard. This standard also contains volumetric property calculations for determining the percent air voids

Asphalt Pavement Analyzer (APA)

The APA was used to evaluate the rutting of HMA mixtures. The APA testing was completed to comply with the AASHTO TP 63-03: “Standard Method of Test for Determining Rutting Susceptibility of Asphalt Paving Mixtures.” The specimens created using the SGC were loaded into molds that hold the specimens under a pressurized hose. A loaded wheel is placed on the pressurized linear hose, which sits on the test specimens and then is tracked back and forth to induce rutting. Test temperatures for the APA are conducted at expected maximum pavement temperature. Wheel load and hose pressure were 445 N and 690 KPa (100 lb. and 100 psi), respectively. The testing in the APA was carried out to 8,000 cycles. The results for the APA rutting tests should not exceed 12.5 mm. The table below lists the rutting data for each HMA specimen.

Table 7: HMA Specimen Rut Depths

Specimen ID At Each Nanoclay Content	PG 64-34 Average APA Rut Depth at Each Nanoclay Content			
	0% (Control)	1%	3%	5%
1	4.033	2.997	3.399	2.246
2	4.460	3.286	2.625	3.815
3	3.705	8.521	3.188	3.711
Specimen ID At Each Nanoclay Content	PG 64-28 Average APA Rut Depth at Each Nanoclay Content			
	0% (Control)	1%	3%	5%
1	6.607	5.544	4.645	3.510
2	5.685	3.986	5.251	3.544
3	6.773	5.559	5.454	2.551
Specimen ID At Each Nanoclay Content	PG 58-34 Average APA Rut Depth at Each Nanoclay Content			
	0% (Control)	1%	3%	5%
1	3.982	3.982	3.425	4.445
2	5.982	5.982	4.090	2.820
3	5.394	5.394	4.831	3.063
Specimen ID At Each Nanoclay Content	PG 58-28 Average APA Rut Depth at Each Nanoclay Content			
	0% (Control)	1%	3%	5%
1	4.176	8.893	3.690	3.290
2	7.559	7.436	5.713	2.437
3	5.817	4.507	6.031	2.896

Data Analysis

The results for DSR rutting resistance were recorded as the failure temperature of the asphalt binder. The failure temperature of asphalt binder corresponds to the temperature at which the Superpave rutting parameter is equal to one Pascal for unaged binders. Tabular results of the failure temperature show the change in failure temperature due to addition of nanoclay. These results were averaged for five tests to create a statistical data set. The averages of the failure temperature were compared to determine changes due to addition of nanoclay.

The results for the DSR low temperature rheological properties were recorded graphically in the form of storage modulus master curves. The storage modulus represents the real portion of the complex shear modulus. The storage modulus is the stiffness of asphalt binders. Analyzing the graphs visually will show the changes to the storage modulus.

The APA rutting results of the rut depth of each specimen are shown graphically. These graphs do not show if the increase in rutting resistance is due to compaction or nanoclay concentration. Graphs showing rutting depth versus nanoclay percentage and rutting depth versus gyratory compaction number were used with linear correlation to determine the strongest correlation and therefore the most likely cause of the increased rutting resistance. The results of this study can be observed in the next section.

CHAPTER IV

RESULTS AND DISCUSSION

Effect of Nanoclay on High Temperature Binder Grade

The goal of this research was to improve the rutting resistance of asphalt binders. The following tables show the DSR failure temperature results of adding the Cloisite 20 nanoclay to asphalt binders. All binder went through the mixing procedure regardless if any nanoclay was added to the binder. This was done to keep a consistent preparation procedure to eliminate error in the data.

The DSR failure temperature for the base PG 64-34 binder showed the greatest increase in high temperature failure when the nanoclay content was increased from 3% to 5%. The test results showed little improvement when only adding 1% nanoclay. This may be due to improper dispersion of the nanoclay in the binder. It is assumed that the nanoclay is well dispersed through the binder. No testing has confirmed the nanoclay content for this research. The modified binder sample may not have actually contained well dispersed nanoclay at 1% by weight of the sample. This is also true for the 3% and 5% nanoclay modified binders; the actual nanoclay content may vary from what is specified.

Table 8: PG 64-34 Failure Temperature

Specimen ID at Each Nanoclay Content	PG 64-34 Failure Temperature at Each Nanoclay Content (°C)			
	0% (Control)	1%	3%	5%
1	69.44	70.03	69.72	72.95
2	70.59	69.5	70.17	72.77
3	69.09	69.91	69.81	72.79
4	70.1	69.39	69.96	73.9
5	69.9	70.14	70.26	72.33
6	69.63			72.48
Average:	69.79	69.79	69.98	72.87
St. Dev.	0.53	0.33	0.23	0.55
COV (%)	0.75	0.47	0.33	0.76
COV (%) = Coefficient of Variation = St. Dev./Average*100				

With the assumption that the nanoclay is well dispersed through the binder; it can be observed that the failure temperature increased with an increase of nanoclay content for the PG 64-28 binder. As with the PG 64-34 binder the largest jump in failure temperature occurred when the nanoclay content was increased from 3% to 5%.

Table 9: PG 64-28 Failure Temperature

Specimen ID at Each Nanoclay Content	PG 64-28 Failure Temperature at Each Nanoclay Content (°C)			
	0% (Control)	1%	3%	5%
1	69.87	70.53	71.55	73.21
2	70.31	70.72	71.62	72.95
3	69.16	70.15	71.54	73.11
4	69.51	70.14	71.29	73.59
5	69.82	70.07	71.22	73.39
6	69.89			
Average:	69.76	70.32	71.44	73.25
St. Dev.	0.39	0.29	0.18	0.25
COV (%)	0.56	0.41	0.25	0.34
COV (%) = Coefficient of Variation = St. Dev./Average*100				

The results for the base PG 58-34 binder do not follow the results for the PG 64 binders. The control binder tested higher in failure temperature than the nanoclay modified samples, with the exception of the 5% nanoclay content sample. The mixing procedure is hypothesized to be responsible for increasing the failure temperature of the control binder. Further investigation into this hypothesis can be found later in Section 4.2. The nanoclay modified specimens show an increase in failure temperature with an increase in nanoclay content. Once again with the largest increase occurring between 3% and 5% nanoclay content

Table 10: PG 58-34 Failure Temperature

Specimen ID at Each Nanoclay Content	PG 58-34 Failure Temperature at Each Nanoclay Content (°C)			
	0% (Control)	1%	3%	5%
1	61.34	59.73	60.52	61.76
2	61.61	60.14	60.61	62.12
3	61.7	60.39	60.67	61.86
4	61.73	60.8	60.27	62.01
5	62.23	60.64	60.72	62
6		60.34		
Average:	61.72	60.34	60.56	61.95
St. Dev.	0.32	0.38	0.18	0.14
COV (%)	0.52	0.63	0.29	0.23
COV (%) = Coefficient of Variation = St. Dev./Average*100				

The results for the base PG 58-28 binder followed the general trend of increasing the failure temperature with an increase in nanoclay content. The largest increase in failure temperature, over all the high temperature DSR testing, occurred when the nanoclay content was increased from 3% to 5%. This large of a jump, 5.57°C is larger than expected when comparing against the other DSR data. It is likely that there is

another factor increasing the failure temperature and not just the increase in nanoclay content.

Table 11: PG 58-28 Failure Temperature

Specimen ID at Each Nanoclay Content	PG 58-28 Failure Temperature at Each Nanoclay Content (°C)			
	0% (Control)	1%	3%	5%
1	65.76	66.17	66.93	72.98
2	65.72	66.32	66.96	72.03
3	67.74	67.17	67.11	72.87
4	65.77	67.76	67.34	72.65
5	65.78	65.83	67.12	72.77
6	65.79	65.73		
7		66.09		
Average:	66.09	66.44	67.09	72.66
St. Dev.	0.81	0.75	0.16	0.37
COV (%)	1.22	1.13	0.24	0.51
COV (%) = Coefficient of Variation = St. Dev./Average*100				

The summary of change in average failure temperature can be observed in the table below.

Table 12: Failure Temperature Summary Data

Difference Between Nanoclay Contents	Difference In Average Failure Temperature: (°C)			
	PG 58-28	PG 58-34	PG 64-28	PG 64-34
0% - 1%	0.35	-1.38	0.56	0
1% - 3%	0.65	0.22	1.12	0.19
3% - 5%	5.57	1.39	1.81	2.89

Investigation into Control Binder Failure Temperature

As stated above the failure temperature of the control PG 58-34 binder performed better, higher failure temperature, than the nanoclay modified binder for the base PG 58-34. It can be observed in the tables below that when the failure temperature was determined for the neat binder, which did not go through the mixing process, the results

were more reasonable and fit the rest of the data. The mixing process is clearly responsible for aging the asphalt binder and therefore the resulting increase in failure temperature. This trend is confirmed with the PG 64-34 0% nanoclay binder.

Table 13: PG 58-34 Failure Temperature (No Mixing)

Specimen ID	Failure Temperature: (°C)	Average: (°C)	St. Dev.
PG58-34-0%-1 NO MIX	61.01	60.34	0.513
PG58-34-0%-2 NO MIX	60.07		
PG58-34-0%-3 NO MIX	59.51		
PG58-34-0%-4 NO MIX	60.64		
PG58-34-0%-5 NO MIX	60.47		

Table 14: PG 64-34 Failure Temperature (No Mixing)

Specimen ID	Failure Temperature: (°C)	Average: (°C)	St. Dev.
PG64-34-0%-1_NO MIX	67.36	67.38	0.363
PG64-34-0%-2_NO MIX	67.57		
PG64-34-0%-3_NO MIX	68.07		
PG64-34-0%-4_NO MIX	66.93		
PG64-34-0%-5_NO MIX	67.19		
PG64-34-0%-6_NO MIX	67.18		

Effect of Nanoclay on Low-Temperature Binder Grade

The hypothesis of this study was that adding nanoclay to the asphalt binder would increase the rutting resistance of the binder. The low temperature rheological properties were investigated to see if the addition of nanoclay will have any effect on the low

temperature properties of the asphalt binders. The following graphs are storage modulus master curves for the asphalt binders.

Storage modulus master curves were created using the Williams-Landel-Ferry (WLF) equation to show the general behavior of the modified and non-modified asphalt binders over wide range of frequencies and temperatures. At low temperatures, physical hardening affects the temperature dependency of asphalt binders. The shear modulus approaches an asymptote, the limiting value referred to as the glass modulus. The glass modulus represents the limiting stiffness attained at high frequencies and low temperatures. The glass modulus typically has a value of 1 GPa. Like stated in the literature review asphalt binders behave like Newtonian fluids at high temperatures. As the slope of the master curve reaches 1:1 viscous flow has been reached and the asphalt is no longer a visco-elastic material.

Figures 3-6 show the storage modulus master curves for the modified and non-modified PG 64-34.

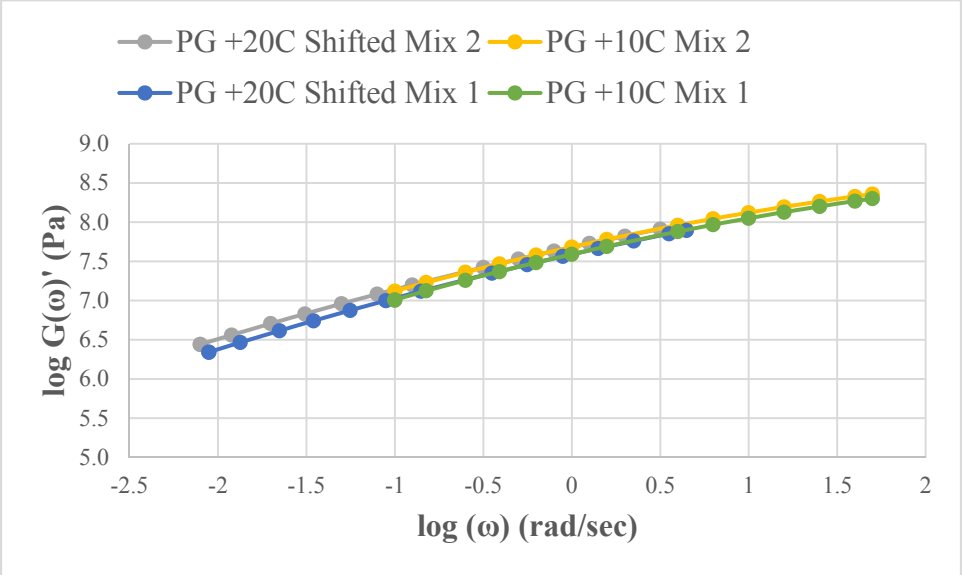

Figure 3: Master Curve: PG 64-34 0% Nanoclay

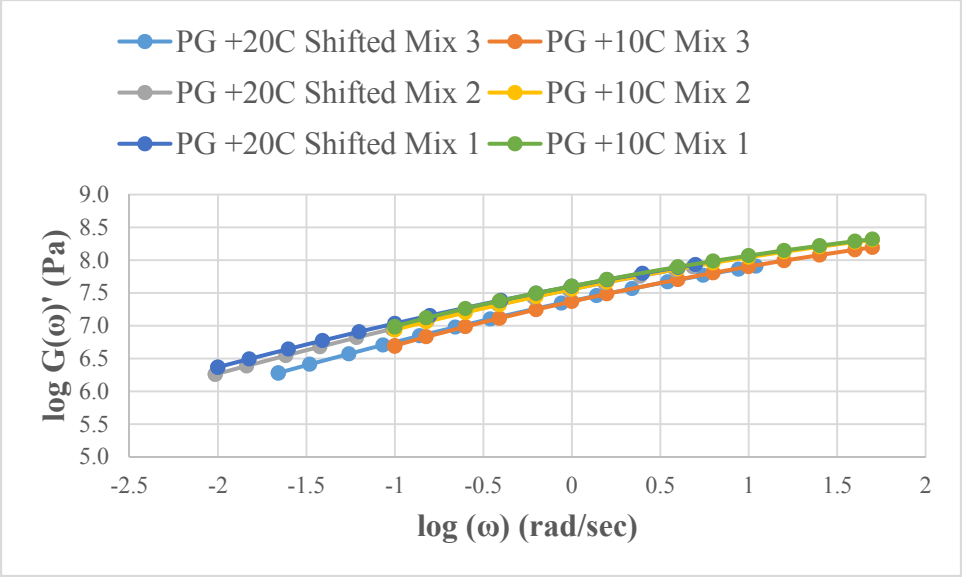

Figure 4: Master Curve: PG 64-34 1% Nanoclay

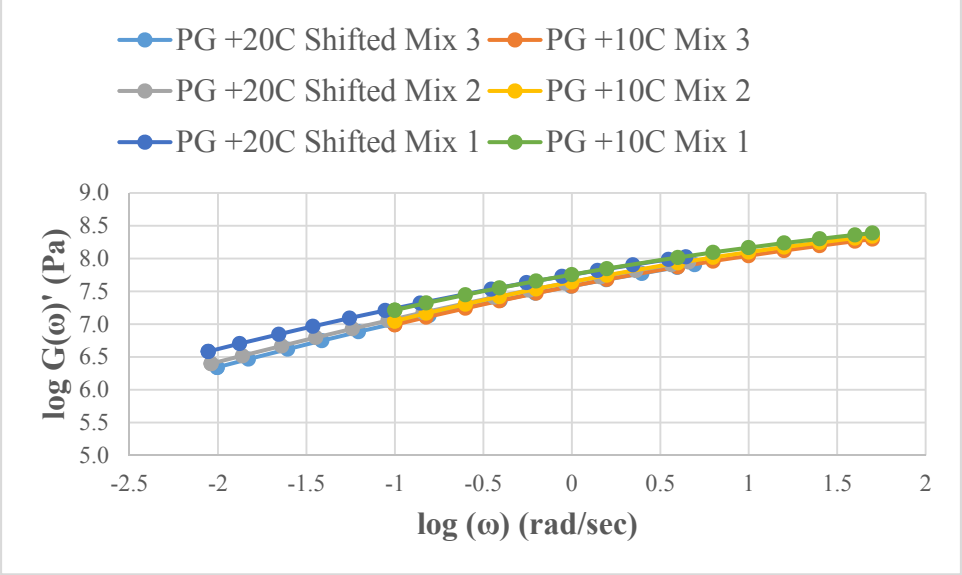

Figure 5: Master Curve: PG 64-34 3% Nanoclay

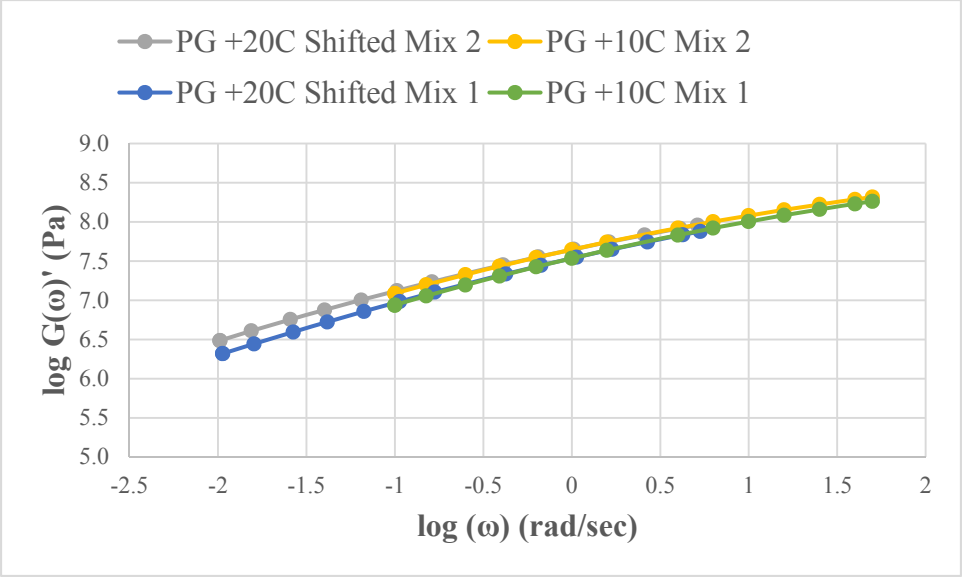

Figure 6: Master Curve: PG 64-34 5% Nanoclay

Figures 7-10 show the storage modulus master curves for the modified and non-modified PG 64-28.

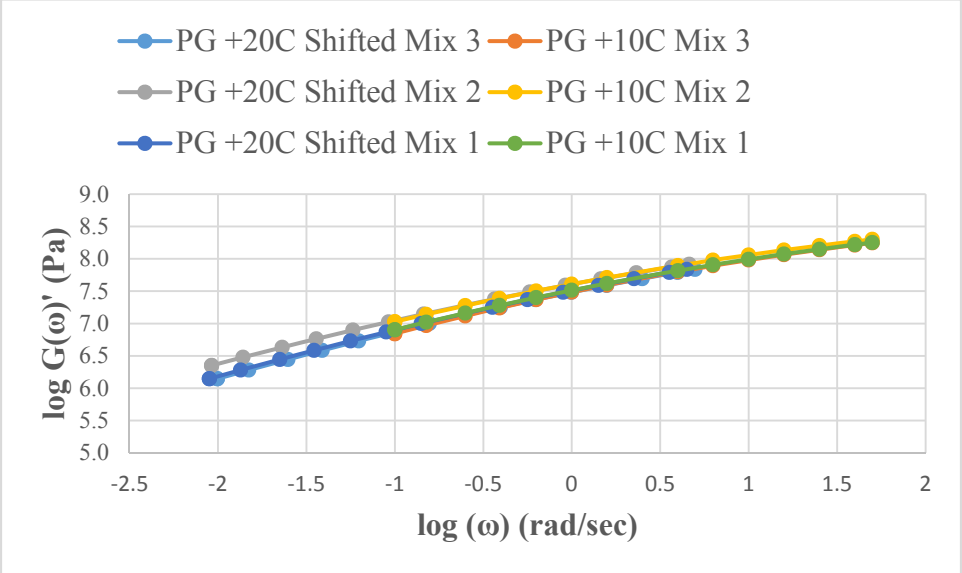

Figure 7: Master Curve: PG 64-28 0% Nanoclay

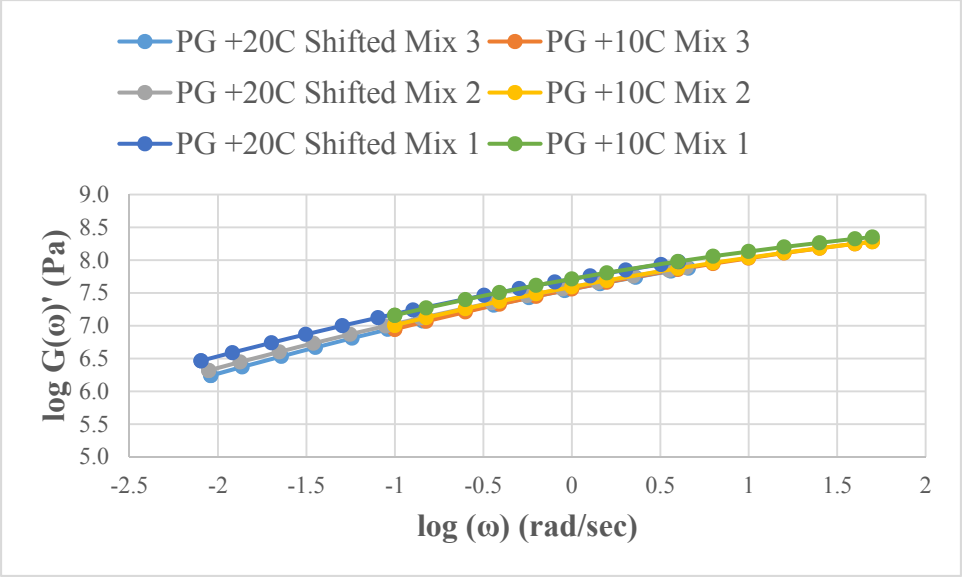

Figure 8: Master Curve: PG 64-28 1% Nanoclay

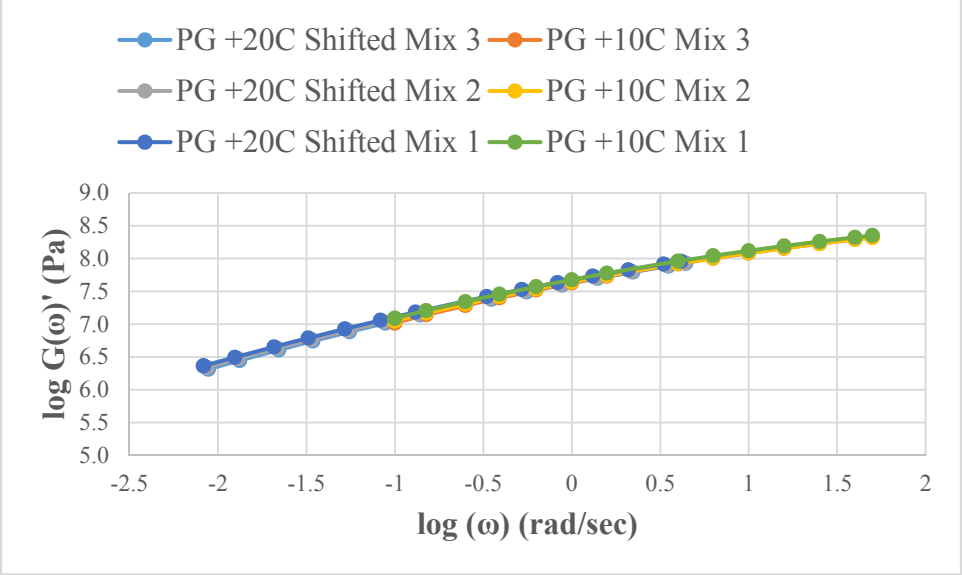

Figure 9: Master Curve: PG 64-28 3% Nanoclay

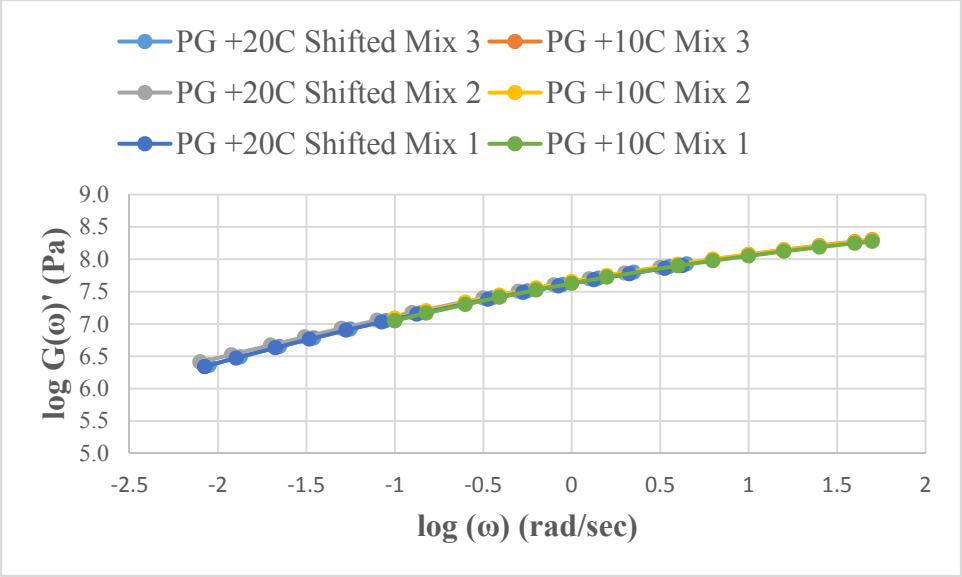

Figure 10: Master Curve: PG 64-28 5% Nanoclay

Figures 11-14 show the storage modulus master curves for the modified and non-modified PG 58-34.

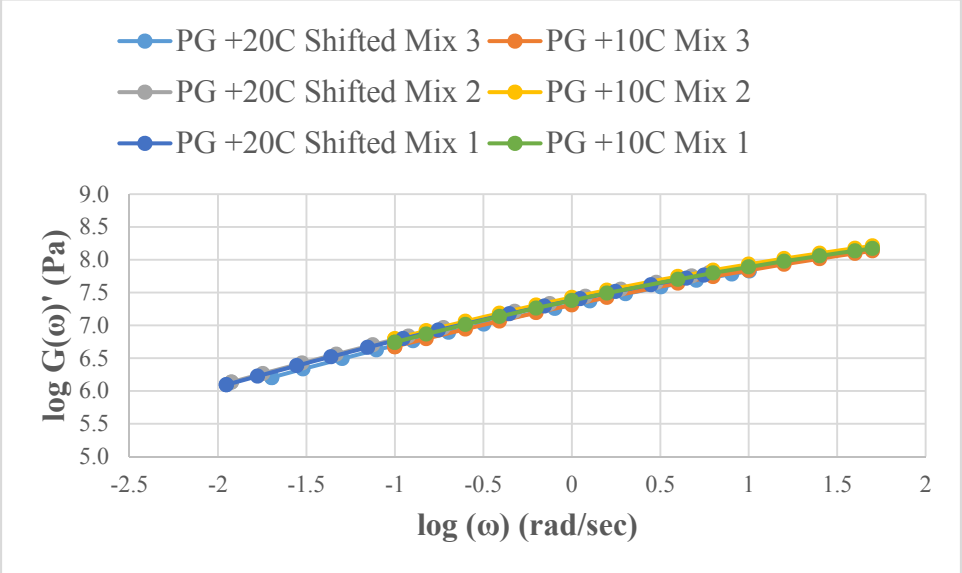

Figure 11: Master Curve: PG 58-34 0% Nanoclay

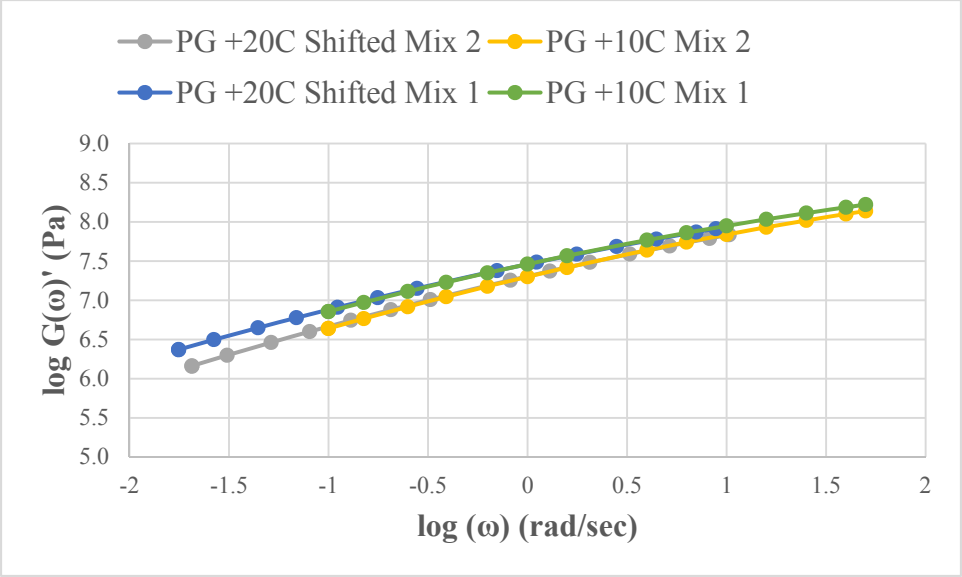

Figure 12: Master Curve: PG 58-34 1% Nanoclay

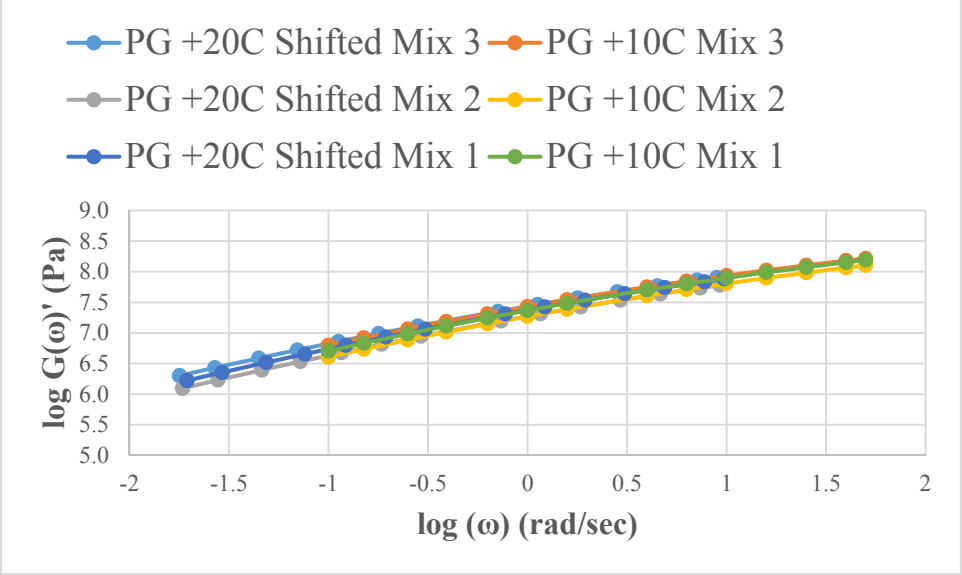

Figure 13: Master Curve: PG 58-34 3% Nanoclay

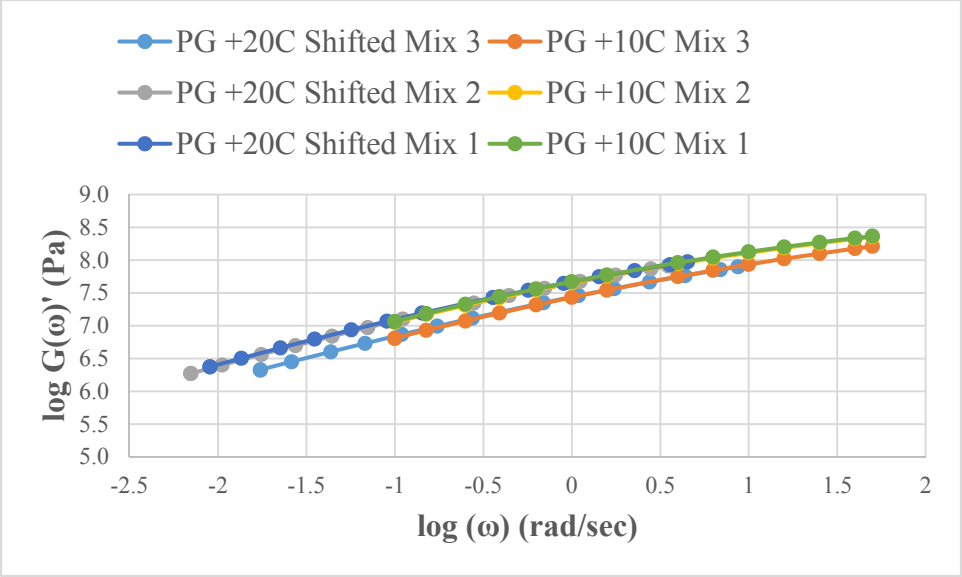

Figure 14: Master Curve: PG 58-34 5% Nanoclay

Figures 15-18 show the storage modulus master curves for the modified and non-modified PG 58-28.

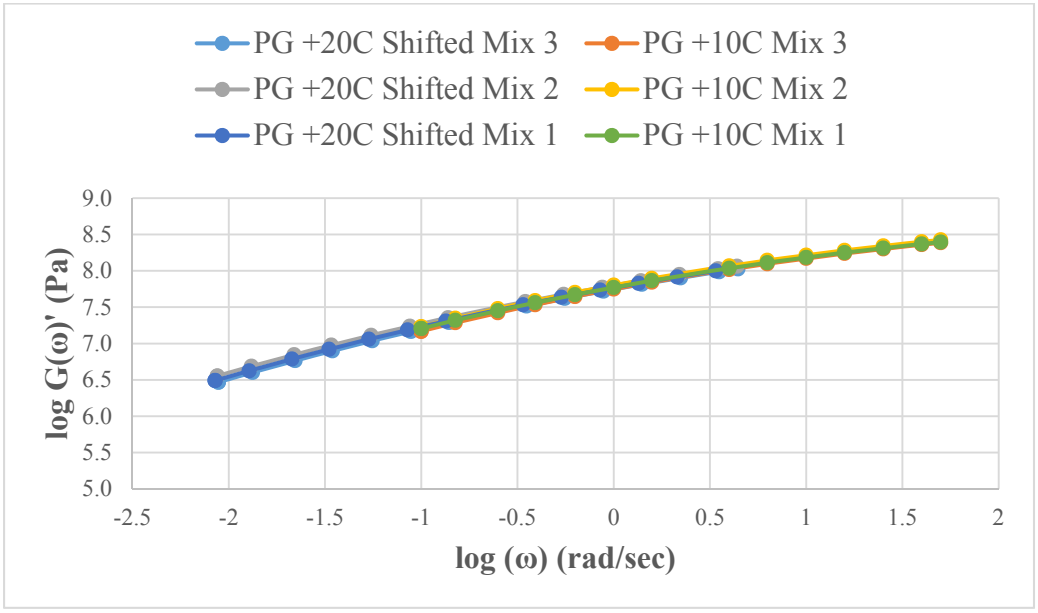

Figure 15: Master Curve: PG 58-28 0% Nanoclay

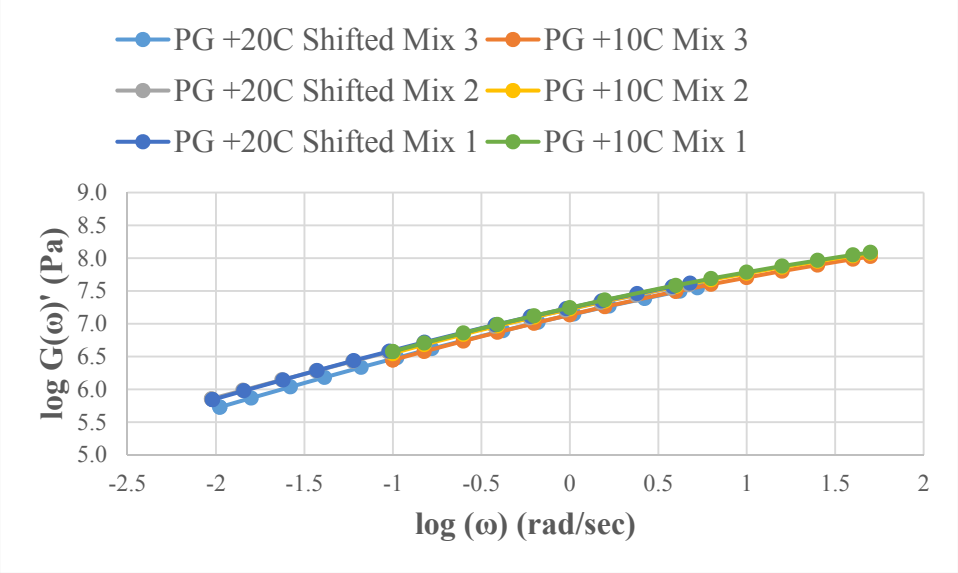

Figure 16: Master Curve: PG 58-28 1% Nanoclay

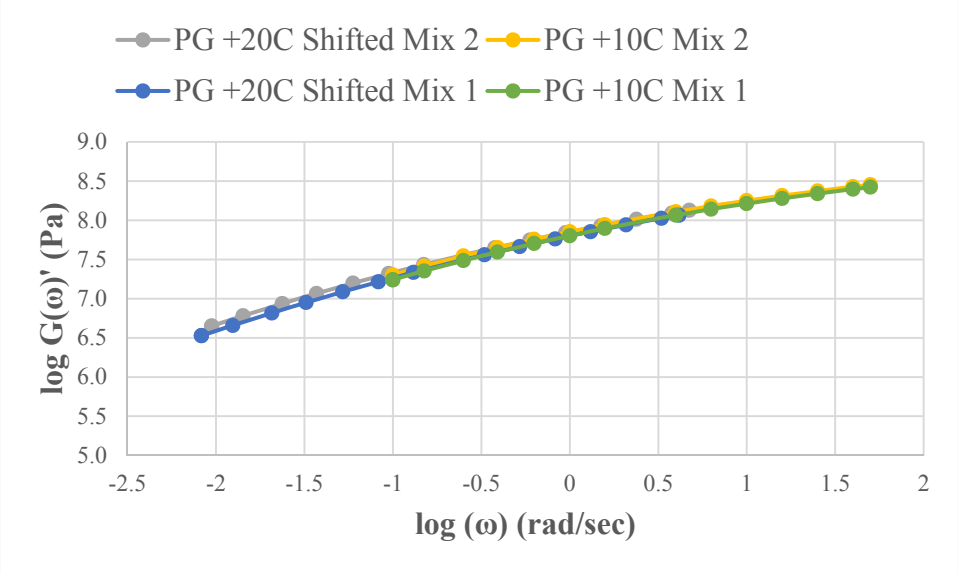

Figure 17: Master Curve: PG 58-28 3% Nanoclay

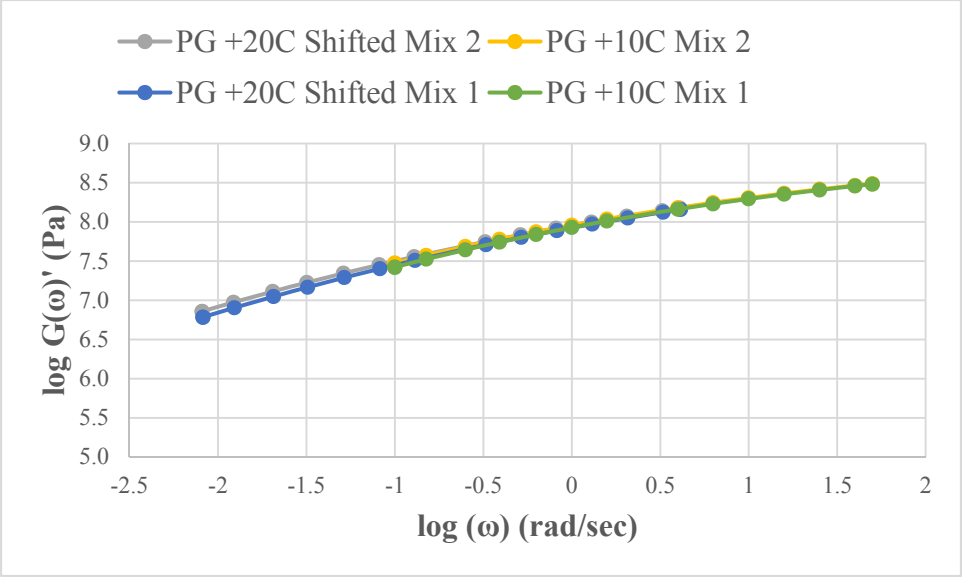

Figure 18: Master Curve: PG 58-28 5% Nanoclay

Further data analysis of the complex shear modulus and phase angle are provided in tables 15-22.

Table 15 shows the summary results for change in low temperature complex modulus for PG 58-28 binder. The results show that the complex modulus values decreased with the addition of 1% nanoclay compared to no nanoclay. However the addition of 3% nanoclay increased the binder stiffness. The 5% nanoclay binder had a higher stiffness at -28°C than the control binder but was less stiff than the 3% nanoclay binder.

Table 15: PG 58-28 Complex Modulus Summary Data at -28°C

Average Low-Temp Results PG 58-28 @ -28°C			
Nanoclay Content	Complex Modulus		
	Average Value (KPa)	St. Dev.	COV (%)
0%	262,425	8,486	3.23%
1%	128,571	9,739	7.57%
3%	300,157	10,212	3.40%
5%	286,092	41,166	14.39%

The phase angle results show the inverse relationship between phase angle and complex modulus. The complex modulus decreased with the addition of 1% nanoclay. The phase angle increased with the addition of 1% nanoclay. This shows that the binder became more elastic with the addition of nanoclay. The opposite trend is observed with the addition of 3% nanoclay. The phase angle decreased and the complex modulus increased.

Table 16: PG 58-28 Phase Angle Summary Data at -28°C

Average Low-Temp Results PG 58-28 @ -28°C			
Nanoclay Content	Phase Angle		
	Average Value (°)	St. Dev.	COV (%)
0%	24.06	1.613	6.70%
1%	34.26	1.956	5.71%
3%	22.38	1.592	7.11%
5%	22.80	1.826	8.01%

Tables 17-18 show the low-temperature summary results for PG 58-34. Unlike the PG 58-28 binder, the complex modulus results for PG 58-34 show a trend to how the nanoclay is affecting the low temperature properties of the binder. The addition of 1% nanoclay increased the stiffness more than the addition of 3% nanoclay and the addition of 5% nanoclay increased the binder stiffness the most. However, independent t-tests show that there is not a significant difference between the results for 1% nanoclay and 3% nanoclay. With this information it can be observed that the addition of nanoclay did significantly increase the binder stiffness at the performance grade low temperature of -28°C. The phase angle results are shown in Table 18. The results show an inverse relationship between phase angle and nanoclay content. The table shows that the addition of nanoclay lowered the phase angle of the binder.

Table 17: PG 58-34 Complex Modulus Summary Data at -34°C

Average Low-Temp Results PG 58-34 @ -34°C			
Nanoclay Content	Complex Modulus		
	Average Value (KPa)	St. Dev.	COV (%)
0%	131,989	5,989	4.54%
1%	163,262	22,412	13.73%
3%	154,328	15,612	10.12%
5%	185,316	23,559	12.71%

Table 18: PG 58-34 Phase Angle Summary Data at -34°C

Average Low-Temp Results PG 58-34 @ -34°C			
Nanoclay Content	Phase Angle		
	Average Value (°)	St. Dev.	COV (%)
0%	34.50	1.976	5.73%
1%	32.25	2.871	8.90%
3%	32.75	2.511	7.67%
5%	31.11	2.737	8.80%

The test results for PG 64-28 also do not show a trend as to how the nanoclay is affecting the low-temperature rheological properties of the binder. Tables 19-20 show the complex modulus and phase angle summary results. Table 19 shows that the addition of nanoclay increased the binder stiffness with the addition of 1% and 3% nanoclay. However, unlike PG 58-28 the addition of 1% nanoclay increased the binder stiffness the most. Independent t-test show that there is not a significant difference between the control binder stiffness and the stiffness of the 5% nanoclay modified binder.

Table 19: PG 64-28 Complex Modulus Summary Data at -28°C

Average Low-Temp Results PG 64-28@ -28°C			
Nanoclay Content	Complex Modulus		
	Average Value (KPa)	St. Dev.	COV (%)
0%	201,999	22,890	11.33%
1%	240,179	56,078	23.35%
3%	216,304	9,747	4.51%
5%	195,098	25,652	13.15%

The phase angle results show that the addition of nanoclay significantly lowered the phase angle for all nanoclay contents. The independent t-tests confirmed that there is a significant difference between the control and nanoclay modified binders.

Table 20: PG 64-28 Phase Angle Summary Data at -28°C

Average Low-Temp Results PG 64-28@ -28°C			
Nanoclay Content	Phase Angle		
	Average Value (°)	St. Dev.	COV (%)
0%	28.05	2.40	8.55%
1%	26.54	3.16	11.91%
3%	27.18	1.67	6.15%
5%	26.44	2.06	7.79%

Tables 21-22 show the complex modulus and phase angle results for PG 64-34. The complex modulus results show that the addition of nanoclay significantly modified the low-temperature binder stiffness. This was confirmed with the independent t-test. However the addition of 1% and 5% nanoclay lowered the stiffness compared to the control binder and the addition of 3% nanoclay increased the stiffness. These results are confirmed with the phase angle results in Table 22.

Table 21: PG 64-34 Complex Modulus Summary Data at -34°C

Average Low-Temp Results PG 64-34@ -34°C			
Nanoclay Content	Complex Modulus		
	Average Value (KPa)	St. Dev.	COV (%)
0%	186,457	18,473	9.91%
1%	174,666	21,752	12.45%
3%	198,769	13,029	6.55%
5%	158,996	31,112	19.57%

Table 22: PG 64-34 Phase Angle Summary Data at -34°C

Average Low-Temp Results PG 64-34@ -34°C			
Nanoclay Content	Phase Angle		
	Average Value (°)	St. Dev.	COV (%)
0%	30.42	2.35	7.72%
1%	32.15	2.62	8.14%
3%	29.31	2.33	7.95%
5%	30.65	4.05	13.21%

Table 23 shows the independent t-test results for the low-temperature DSR testing.

Table 23: Independent t-test: Effect of Nanoclay on Different Binder Grades

Complex Modulus																
Nanoclay Content	PG 58-28				PG 58-34				PG 64-28				PG 64-34			
α = 0.05	0%	1%	3%	5%	0%	1%	3%	5%	0%	1%	3%	5%	0%	1%	3%	5%
0%	-	Y	Y	Y	-	Y	Y	Y	-	Y	Y	N	-	Y	Y	Y
1%	-	-	Y	Y	-	-	N	Y	-	-	Y	Y	-	-	Y	Y
3%	-	-	-	N	-	-	-	Y	-	-	-	Y	-	-	-	Y
Phase Angle																
Nanoclay Content	PG 58-28				PG 58-34				PG 64-28				PG 64-34			
α = 0.05	0%	1%	3%	5%	0%	1%	3%	5%	0%	1%	3%	5%	0%	1%	3%	5%
0%	-	Y	Y	Y	-	Y	Y	Y	-	Y	Y	Y	-	Y	Y	N
1%	-	-	Y	Y	-	-	N	N	-	-	N	N	-	-	Y	Y
3%	-	-	-	N	-	-	-	Y	-	-	-	Y	-	-	-	Y
"Y" -There is a significant difference "N" -There is not a significant difference																

All but one of the low-temperature DSR tests showed significant difference from the control binder but only PG 58-34 showed any significant trend of change of complex modulus with change in nanoclay content.

Effect of Nanoclay on Rutting Resistance of HMA Specimens

The APA was used to determine if the nanoclay had a similar effect on the asphalt pavement specimens as it did on the asphalt binders. The following table has the average rut depths for the asphalt pavement specimens after the 8,000 cycle loading was complete. The following summary table shows the average rut depth for the three HMA specimens created for each binder group.

Table 24: APA Rut Depth Summary

Nanoclay Content	Average Rut Depth @ 8,000 APA Cycles (mm)			
	PG 58-28 @58°C	PG 58-34 @58°C	PG 64-28 @64°C	PG 64-34 @64°C
0%	5.851	4.844	6.355	4.066
1%	6.945	5.120	5.030	4.934
3%	5.145	4.115	5.117	3.071
5%	2.874	3.443	3.202	3.257

As Table 24 shows that the addition of nanoclay generally reduces rut depth with the greatest reduction happening with the 5% nanoclay content. Individual t-tests results are shown in Table 25.

Table 25: Independent t-test: Effect of Nanoclay on Rutting Depth

Nanoclay Content	Rutting Depth @ 8,000 Cycles															
	PG 58-28				PG 58-34				PG 64-28				PG 64-34			
$\alpha = 0.05$	0%	1%	3%	5%	0%	1%	3%	5%	0%	1%	3%	5%	0%	1%	3%	5%
0%	-	N	N	Y	-	N	N	N	-	Y	Y	Y	-	N	Y	N
1%	-	-	N	Y	-	-	Y	N	-	-	N	Y	-	-	N	N
3%	-	-	-	Y	-	-	-	N	-	-	-	Y	-	-	-	N

There is no significant difference between the control binder and 1% nanoclay except for PG 64-28. Rut depth of the control binder is significantly different than HMA specimens containing 5% nanoclay for binders PG 58-28 and PG 64-28. Even though the rut depth summary table shows that all the HMA specimens with 3% and 5% nanoclay have lower average rut depth than the control binder, only rut depth for PG 58-28 and PG 64-28 is significantly different at the 5% significance level.

Effect of Air Voids on Rut Depth of HMA Specimens

The following figures show the relationship of air voids and rut depth

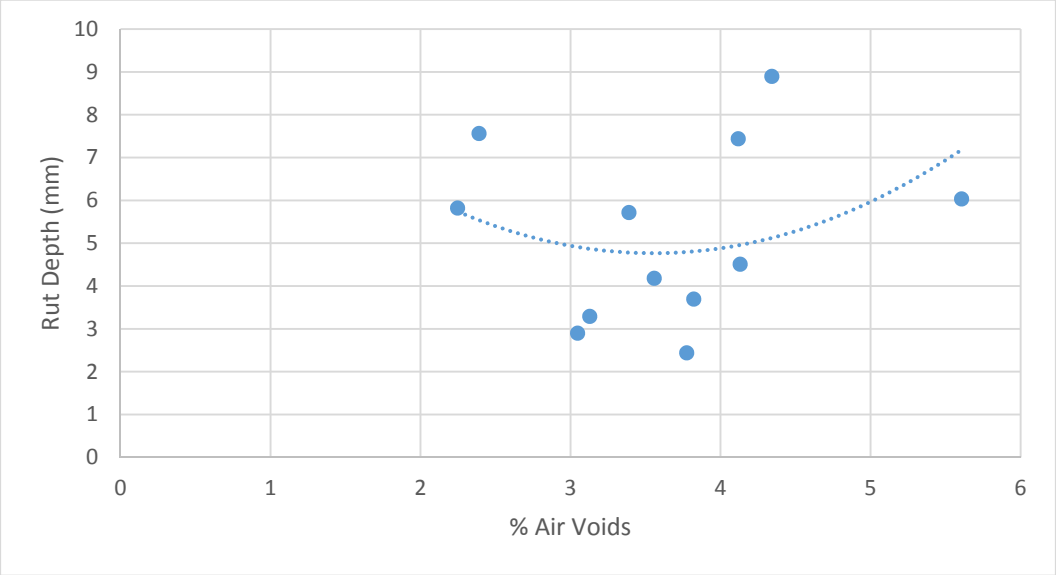

Figure 19: PG 58-28 Air Voids vs Rut Depth

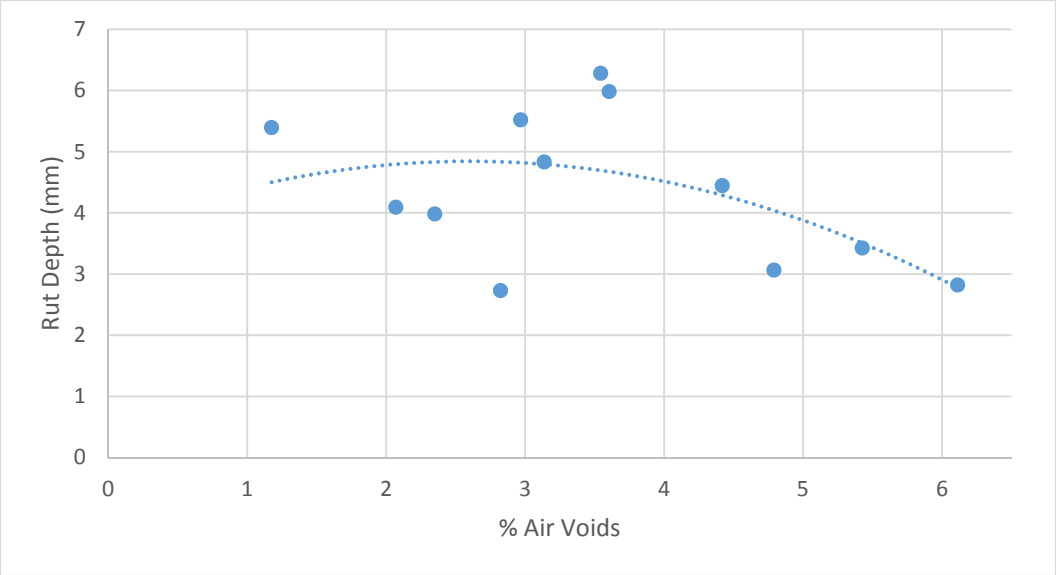

Figure 20: PG 58-34 Air Voids vs Rut Depth

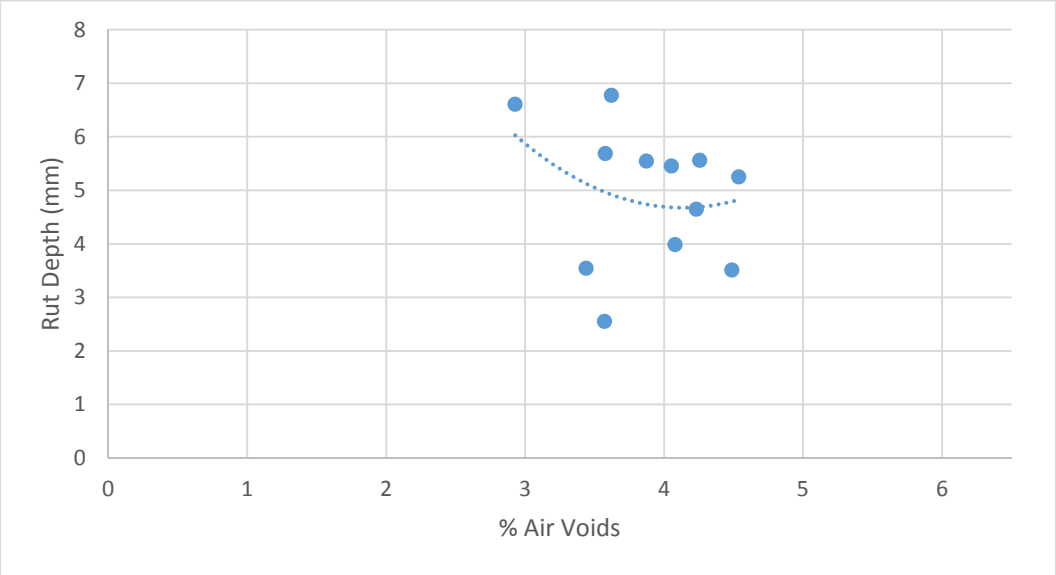

Figure 21: PG 64-28 Air Voids vs Rut Depth

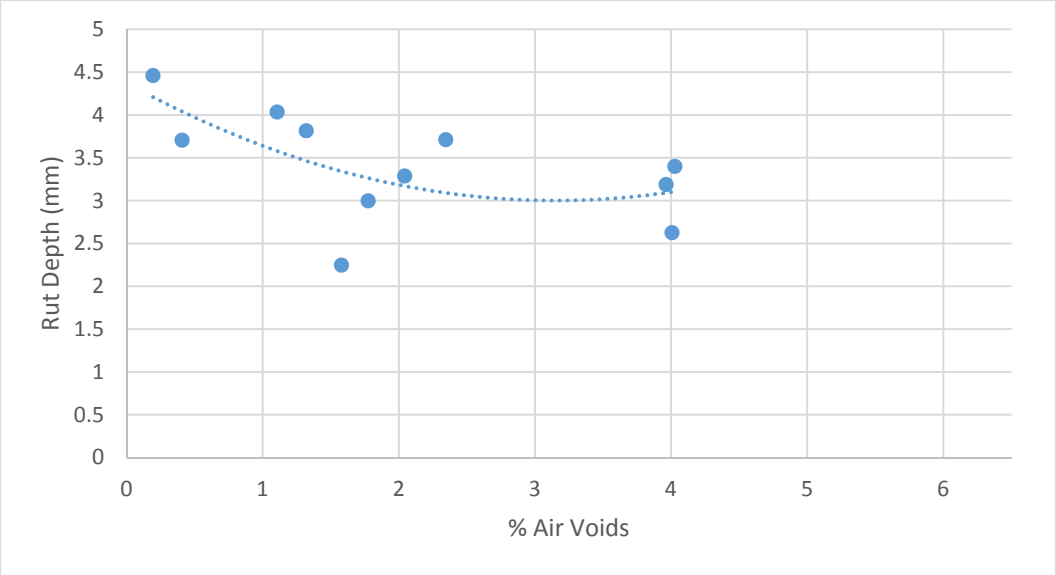

Figure 22: PG 64-34 Air Voids vs Rut Depth

It can be observed that there is not a strong correlation between air voids and rut depth of the HMA specimens. It is generally expected that high air voids will lead to rutting of the pavement. The results for PG 58-34 have a negative second order polynomial regression suggesting that as the air voids increase the rut depth will decrease.

CHAPTER V

CONCLUSIONS

Nanoclay Improved Rutting Resistance of Asphalt Binders

The high performance grade temperature DSR research determined that the addition of nanoclay to the base binder improved the rutting resistance. The nanoclay improved the stiffness of the binders and made the binders more resistance to deformation at high temperatures.

Mixing Procedure Aged the Binder

The investigation into the magnitude of the control binder failure temperature revealed that the mixing procedure performed in this research resulted in aging of the binder. Mixing the binder and nanoclay in a controlled environment will minimize the oxidation and loss of volatile components of the binder. This will allow for more informative results as to the magnitude of increase in rutting resistance due to the nanoclay modification alone.

Nanoclay Reduced the Low-Temperature Cracking Resistance of Binders

The low-temperature DSR testing produced less than desirable results. The results were difficult to decipher due to fluctuation in results. The PG 58-34 results were the most consistent and statistically significant. The determination that the stiffness increased at low temperatures was based on these test results.

Nanoclay Improved the Rutting Resistance of HMA Specimens

The addition of nanoclay to the asphalt binder increased the rutting resistance of the HMA specimens. Generally, the average rutting depth decreased with an increase of nanoclay. However, not all of the results were significant at the 5% level.

CHAPTER V

RECOMMENDATIONS

Further investigation into the proper mixing procedures and equipment should be considered to determine the validly of the data collected in this research. The mixing should be should be done in a controlled environment to eliminate the increase in stiffness due to aging during mixing and show the true effects of nanoclay modification.

After a proper mixing procedure is determined; additional low-temperature DSR testing should be conducted to determine the effects of nanoclay on the fatigue and cracking resistance of the nanoclay modified binders.

Creating complex modulus master curves with the Christensen-Anderson-Marasteanu (CAM) model. The master curves created in this research were modeled after an example procedure provided by Sui et al 2010 using the WLF equation. The CAM model is widely used by other researchers and is needed to compare results over a frequency and temperature range.

Additional HMA should be analyzed using the APA using a consistent HMA mix design so that the APA results can be compared and contrasted for all performance grade binders.

Further DSR testing using Rolling Thin Film Oven (RTFO) and Pressure Aging Vessel (PAV) aged binders would provide additional information on the long term benefits of nanoclay modification and would better represent the rheological properties after short term aging

CHAPTER VI

APPENDIX

Aggregate Sieve Analysis

Agg: A "Strata Crusher Dust"		
Sieve Size	Sieve Size No.	Percent Passing
9.5 mm	3/8"	99.74%
4.75 mm	No. 4	88.01%
2.36 mm	No. 8	67.20%
1.18 mm	No. 16	45.99%
0.60 mm	No. 30	27.95%
0.30 mm	No. 50	11.32%
0.15 mm	No. 100	5.72%
Pan		0.00%

Agg: B "Strata Natural Sand"		
Sieve Size	Sieve Size No.	Percent Passing
9.5 mm	3/8"	100.00%
4.75 mm	No. 4	99.72%
2.36 mm	No. 8	98.66%
1.18 mm	No. 16	91.64%
0.60 mm	No. 30	67.26%
0.30 mm	No. 50	23.60%
0.15 mm	No. 100	4.84%
Pan		0.00%

Agg: D "Strata Crushed Rock"		
Sieve Size	Sieve Size No.	Percent Passing
25 mm	1"	100.00%
19 mm	3/4"	100.00%
12.5 mm	1/2"	92.26%
9.5 mm	3/8"	67.67%
4.75 mm	No. 4	6.27%
2.36 mm	No. 8	1.74%
Pan		0.00%

Agg: F "Fines From Lab"		
Sieve Size	Sieve Size No.	Percent Passing
9.5 mm	3/8"	100.00%
4.75 mm	No. 4	100.00%
2.36 mm	No. 8	100.00%
1.18 mm	No. 16	99.94%
0.60 mm	No. 30	99.86%
0.30 mm	No. 50	99.46%
0.15 mm	No. 100	96.05%
0.075mm	No. 200	83.38%
Pan		0.00%

Agg: G "Crushed Granite"		
Sieve Size	Sieve Size No.	Percent Passing
25 mm	1"	100.00%
19 mm	3/4"	96.82%
12.5 mm	1/2"	65.73%
9.5 mm	3/8"	41.26%
4.75 mm	No. 4	4.88%
2.36 mm	No. 8	1.09%
1.18 mm	No. 16	0.64%
0.60 mm	No. 30	0.00%
0.30 mm	No. 50	0.00%
0.15 mm	No. 100	0.00%
Pan		0.00%

Agg: H "Green Bucket Crushed Granite"		
Sieve Size	Sieve Size No.	Percent Passing
9.5 mm	3/8"	100.00%
4.75 mm	No. 4	2.94%
2.36 mm	No. 8	0.00%
1.18 mm	No. 16	0.00%
Pan		0.00%

CHAPTER VII

REFERENCES

Airey, G. D., Rahimzadeh, B., & Collop, A. C. (2004). Linear Rheological Behavior of Bituminous Paving Materials. *Journal of Materials in Civil Engineering*.

Anderson, D., Christensen, D., Bahia, H. U., Dongre, R., Sharma, M., Antle, C., & Button, J. (1994). *Binder Characterizatoin and Evaluaion Volume 3: Physical Characterization.* Washington, D.C.: National Research Council.

Bonemazzi, F., Braga, V., Corrieri, R., Giavarini, C., & Sartori, F. (1996). Characteristics of Polymers and Polymer-Modified Binders. *Transportation Research Record*, 36-47.

Huang, Y. H. (2004). *Pavement Analysis and Design.* Upper Saddle River, New Jersey, USA: Pearson Education, Inc.

Marasteanu, M. O. (1999). *Inter-conversions of the Linear Viscoelastic Functions Used for the Rheological Characterization of Asphalt Binders.* Pennsylvania State University.

Marasteanu, M. O., & Anderson, D. A. (2000). *Establishing Linear Viscoelastic Conditions for Asphalt Binders.* Trasportation Research Record.

Miller, John S., and William Y. Bellinger. *Distress Identification Manual for the Long-Term Pavement Performance Program*. No. FHWA-HRT-13-092. 2014.

Nazzal, M. D., Kaya, S., Gunay, T., & Ahmedzade, P. (2012). Fundamental Characterization of Asphalt Clay Nano-Composites. *Journal of Nanomechanics and Micromechanics*, 1-30.

Newman, J. K. (1998). Dynamic Shear Rheological Properties of Polymer Modified Asphalt Binders. *Journal of Elastomers and Plastics*, 245-263.

Onochie, A., Fini, E., Yang, Y., Mills-Beale, J., & You, Z. (2012). *Rheological Characterization of Nano-particle Based Bio-modified Binder.*

Roberts, F. L., Kandhal, P. S., Brown, E. R., Lee, D.-Y., & Kennedy, T. W. (1996). *Hot Mix Asphalt Materials, Mixture Design, and Construction.* Lanham: NAPA Research and Education Foundation.

Struik, L. C. E. *Physical Hardening in Amorphous Polymers and Other Materials.* Elsevier, 1978

Sui, C., Farrar, M. J., Tuminello, W. H., & Turner, T. F. (2010). New Technique for Measuring Low-Temperature Properites of Asphalt Binders with Small Amounts of Material. *Transportation Research Record: Journal of the Transportation Research Board*, 22-28.

Yao, H., You, Z., Li, L., Goh, S. W., Lee, C. H., Yap, Y. K., & Shi, X. (2013). Rheological Properties and Chemical Analysis of Nanoclay and Carbon Microfiber Modified Asphalt with Fourier Transform Infared Spectoscopy. *Construction and Building Materials*, 327-337.

Yu, J.-Y., Feng, P.-C., Zhang, H.-L., & Wu, S.-P. (2009). Effect of Organo-Montmorillonite on Aging Properties of Asphalt. *Construction and Building Materials*, 2636-2640.